Aerospace Science and Technology 114 (2021) 106758

Contents lists available at ScienceDirect

Aerospace Science and Technology

www.elsevier.com/locate/aescte

A fault detection method for FADS system based on interval-valued neutrosophic sets, belief rule base, and D-S evidence reasoning

Qianlei Jia *, Jiayue Hu, Weiguo Zhang

School of Automation, Northwestern Polytechnical University, Xi'an 710072, China

ARTICLE INFO

Article history:
Received 9 March 2020
Received in revised form 23 November 2020
Accepted 19 April 2021
Available online 27 April 2021
Communicated by Xiande Fang

Keywords:
Fault detection
Interval-valued neutrosophic sets (IVNSs)
Belief rule base (BRB)
Dempster-Shafer (D-S) evidence reasoning
Flush air data sensing (FADS)

ABSTRACT

Fault detection, with the characteristics of strong uncertainty and randomness, has always been one of the research hotspots in the field of aerospace. Considering that devices will inevitably encounter various unknown interference in the process of use, which greatly limits the performance of many traditional fault detection methods. Therefore, the main aim of this paper is to address this problem from the perspective of uncertainty and randomness of measurement signal. In information engineering, interval-valued neutrosophic sets (IVNSs), belief rule base (BRB), and Dempster-Shafer (D-S) evidence reasoning are always characterized by the strong ability in revealing uncertainty, but each has its drawbacks. As a result, the three theories are firstly combined in this paper to form a powerful fault detection algorithm. Besides, a series of innovations are proposed to improve the method, including a new score function based on p-norm for IVNSs and a new approach of calculating the similarity between IVNSs, which are both proved by authoritative prerequisites. To illustrate the effectiveness of the proposed method, flush air data sensing (FADS), a technologically advanced airborne sensor, is adopted in this paper. The aerodynamic model of FADS is analyzed in detail using knowledge of aerodynamics under subsonic and supersonic conditions, meanwhile, the high-precision model is established based on the aerodynamic database obtained from CFD software. For further confirming the validity and feasibility, a comparison with the methods based on parity equation, χ^2 distribution, and information fusion method ordered weighted averaging (OWA) with three sets of weight vectors are conducted.

1. Introduction

1.1. Background

In the field of engineering application, fault detection of equipment has always been an unavoidable hot issue. Once the system fails and is not diagnosed timely, it will cause huge economic losses and even death. Take the aviation sector as an example. For Partnair Flight 394, the four bolts used to fix the vertical tail of the aircraft failed, causing the aircraft to disintegrate, all passengers and crew were killed. In 1995, Bergen Airlines Flight 301 crashed. An investigation later revealed that the cause of the huge crash was the failure of pitot tube. Also, it was precisely because of a malfunction in the navigation system that Adam Airlines Flight 574 crashed, causing 102 deaths. Therefore, it is of great significance to ensure that the faults on the equipment are detected in time, which can save many people's lives.

1.2. Related work

In past research, many scholars have carried out research in fault detection [1]. The existing methods can be summarized into the following categories:

1) The methods based on analytical model:

Generally speaking, these methods mainly include filter method [2–5], least squares method [6,7], and equivalent space method [8]. The key thinking of these methods is to calculate the residuals between the actual performance and the expected performance derived

* Corresponding author.
E-mail address: jiaql@mail.nwpu.edu.cn (Q. Jia).

https://doi.org/10.1016/j.ast.2021.106758
1270-9638/

from the analytical model, and then analyze the residuals to determine the fault type. Actually, this kind of method can indeed achieve the fault detection to some extent, but it is greatly affected by the accuracy of model. Once the accuracy of model can not be guaranteed, the final result will absolutely be affected.

2) The methods based on signal processing:

Wavelet analysis: These methods are mainly to carry out wavelet transform on the input and output signals, and make use of the transform to find singularities. Then, remove the extreme points caused by input mutation and the remaining extreme points correspond to the fault state. In [9], wavelet analysis, Fourier transform, and multi-Layer perceptron neural network were combined to design a new fault detection algorithm. In [10], discrete wavelet transform (DWT) was employed to extract the noise from process signal, and then made use of continuous wavelet transform to detect the abrupt fault of process noise signal. In [11], DWT was adopted to detect the dynamics of various failures, and then predict the remaining useful life (RUL) of faulty bearings with adaptive Bayesian.

Empirical mode decomposition (EMD): To obtain intrinsic mode function (IMF), EMD was proposed by Norden E. Huang, the principle of which is to decompose the original signal into several intrinsic modal functions and smooth the non-stationary signal. In [12], an EMD-based approach was used along with artificial neural network (ANN) for the analysis of real-time arc signals. Considering that when multiple faults alongside noisy environment are present together, the performance of the conventional signal processing methods like fast Fourier transform (FFT) are limited. Therefore, ensemble empirical mode decomposition (EEMD) and cyclostationary analysis were connected and applied to the fault detection of wind turbine gearboxes in [13]. To overcome the poor performance in fault detection caused by data inconsistency, convolutional neural networks (CNNs) and variational mode decomposition (VMD) were integrated to form variational mode decomposition with deep convolutional neural networks (VMD-DCNNs) [14]. In VMD-DCNNs, original vibration signals were processed end-to-end without manual experience and manual intervention to achieve the fault detection of rolling bearings.

Spectrum analysis: For this method, the complex signal is decomposed into the sum of finite or infinite spectrum components, and then the power spectrum of each component is calculated to determine the fault type and fault source. In [15], the armature current signal of generator was collected by synchronous sampling method, and the signal was transformed from time domain to frequency domain with FFT. By extracting the characteristic quantity of current signal in frequency domain during normal and fault operation of motor, the frequency component and amplitude of signal were determined for fault detection. To achieve the fault detection of squirrel cage motors, Hilbert spectrum was employed in [16]. Simulation results showed that this method had relatively high accuracy when the levels of damage in the broken bars were of 3 mm, 5 mm and 7 mm. Besides, spectrum analysis was also employed in Tennessee Eastman Process (TEP) [17], gear system [18–20].

Unlike the model-based methods, the methods on the basis of signal processing do not require high-precision models, but the research also gives rise to some difficulties. For example, Fourier analysis is mainly aimed at the smooth signals. However, most fault signals are contained in the transient signals, and the performance of non-stationary dynamic signal will degrade.

3) Knowledge-based methods:

Knowledge-based fault detection methods are a set of intelligent computer programs designed according to people's long-term practical experience and a large number of fault information, the characteristic of which is that the precise mathematical model of the object is not required. The specific methods can be divided into the following categories.

Expert system: In [21], rule base and case base for the fault detection of expert system was established based on the domain expert knowledge and relevant fault cases of turbine generator sets. In [22], rule-based expert system was applied to the fan fault detection. To overcome the shortcomings of time-consuming and difficult convergence of back propagation neural network expert system (BPES), a novel multi-BP expert system (MBPES) method for power system fault detection was proposed in [23]. Moreover, expert system was also combined with many other methods for troubleshooting, including fault tree [24–26], genetic algorithm (GA) [27], and fuzzy reasoning [28,29]. However, although expert system has the ability to deal with the problem regardless of the accuracy of model, there is much room for improvement in reducing computation.

Fuzzy logic: The main purpose of this method is to overcome the difficulties caused by the uncertainty, imprecision and noise. Therefore, it shows the advantages in dealing with large time delay, time-varying, and nonlinear problem. In [30], a fuzzy neural network model suitable for fault detection was established based on the combination of fuzzy theory and neural network. In the method, a fuzzy inference algorithm was achieved and the fuzzy neural network learning weights were converted into case-based reasoning-based diagnostic guidance operators. In [31], Thumati developed a multiple model prognosis method based on the fuzzy logic for a two-tank system.

D-S evidence reasoning: In [32], a joint fault detection method based on D-S evidence reasoning was proposed. The output of each sub filter was taken as evidence, and the joint fault detection function was established by using the state estimation value and error covariance of each sub filter. The fault detection of each navigation system was realized by fusing multiple evidences. In [33], D-S evidence reasoning and radial basis function (RBF) were combined to address the computational combinatorial explosion problem. The improved algorithm was successfully applied to the fault detection of underground sensors. Considering the advantages of rough set in extracting key information and D-S evidence reasoning in conflict information processing, a new fault detection algorithm was proposed in [34]. Besides, long short-term memory networks (LSTM), convolutional neural network (CNN) and random forests (RF) were adopted to conclude the fault features, and then D-S evidence reasoning was employed to fuse the information and identify the fault type [35]. Due to the ability of D-S evidence reasoning in expressing uncertain information, it has also been applied in many other fields [36–38].

Support vector machine (SVM): SVM is a learner suitable for high-dimensional and small sample data classification based on statistical learning theory, which occupies an important part in fault detection. In [39], chaos particle swarm optimization algorithm and SVM were combined to propose a new algorithm for the fault detection problem of wireless sensor. To further improve SVM, particle swarm optimization (PSO) algorithm was employed to train SVM [40,41]. In [42], with strong global search capability of bacterial foraging algorithm (BFA), the optimization method—support vector machine parameters optimization based on bacterial foraging algorithm was proposed. Although the solution of SVM is a convex quadratic programming problem and there is a unique solution when the model structure and model parameters are determined. However, due to the limitation of computational memory, when the number of fault feature samples is large, SVM can not be trained or the training speed is very slow. Therefore, how to train SVM with large sample set is a bottleneck problem in practical application. Besides, how to select the model structure and parameters to obtain the optimal fault diagnosis results is also a thorny problem.

4) The methods based on artificial intelligence:

Genetic algorithm (GA): The algorithm mainly reorganizes individuals with a certain structural form in the group through genetic operations to continuously approach the optimal solution. Aiming at the characteristics of transformer fault types, a fault detection algorithm was proposed based on GA to optimize weights and thresholds between input layer and hidden layer [43]. Considering that GA possesses a high performance in global search, it was combined with the tabu search algorithm characterized by good local search ability to form genetic algorithm-Tabu search (GATS) in [44], and the newly proposed algorithm was used to address the fault detection of power systems. Furthermore, GA was also adopted to deal with the fault detection of analog filter circuit [45], floating disc system [46], reciprocating compressor [47], and wind turbine gearbox [48]. However, the algorithm is difficult to deal with the problems with high dimension. Besides, the limited ability to explore new spaces and poor stability are also the shortcomings of GA.

Ant colony optimization (ACO): ACO is a probabilistic algorithm used to find the optimal path in a graph. It is characterized by positive feedback and distributed collaboration. In [49], the state recognition problem of mechanical fault detection was transformed into a clustering problem of different states, and then a distance-based detection method was proposed using ant colony algorithm, which distinguished the mechanical state by comparing distances. In [50], ACO and SVM were combined to obtain a new algorithm ACO-SVM, the feasibility of which was illustrated by the fault detection of locomotive roller bearings. To eliminate the interference of high-dimensional and improve the fault detection ability of SVM, a new quantum ant colony optimization (QACO) algorithm was proposed in [51]. In the field of fault detection, ACO is a widely used algorithm with strong robustness and excellent integration with other methods. Nevertheless, the slow convergence speed and easy to fall into local optimum are two inevitable shortcomings of the algorithm.

Particle swarm optimization (PSO): To propose a new approach for fault detection and isolation (FDI) on industrial systems, PSO and ACO were adopted comprehensively in [52]. In [53], the influence of particle number, accelerate constant, inertia weight, and maximum limited velocity on PSO was studied emphatically, and then PSO with dynamic parameters was applied on the neural network training for gearbox fault detection. Besides, a new algorithm of regrouping particle swarm optimization-based neural network (RegPSONN) was formed on the basis of PSO and neural network for rolling bearing fault detection [54]. Similarly, PSO and neural network were integrated to solve the fault detection of analog circuit in [55]. However, due to the lack of dynamic speed adjustment, the method is prone to falling into the local optimum, resulting in low convergence accuracy. In addition, how to select the appropriate parameters to achieve the optimal effect is also a problem to be studied.

1.3. Innovations

After sorting out a large number of relevant literatures, it can be found that there are still some research gaps on the fault detection. The key contributions of this study can be summarized as follows:

1) Taking into account that due to the presence of various interferences, measurement result of equipment will fluctuate up and down, showing strong uncertainty and randomness. To address the problem, interval-valued neutrosophic sets (IVNSs), a powerful platform in expressing uncertain information, is firstly integrated with belief rule base (BRB) and D-S evidence reasoning to propose a novel fault detection algorithm in this paper.
2) Two critical steps for the proposed algorithm are to calculate the similarity between IVNSs and design a convincing score function. After analyzing the previous relevant studies, a new approach for calculating the similarity based on implication operator is derived, and the rationality is proved by the theorem. In addition, to quantify the information contained in different IVNSs, a score function on the basis of p-norm in mathematics is proposed in this paper.
3) Until now, there has been no systematic research on the fault detection of flush air data sensing (FADS) system except two methods: 1) Parity equation: This method [56] takes the system model as the starting point and deduces the standard fault vector table through the mathematical formula to achieve the purpose of fault detection. However, the study of the method gives rise to a main difficulty: Limited by the variance of measurement noise. Once the variance of noise increases, the vibration amplitude of data will increase and the accuracy of this method will be greatly affected. 2) χ^2 distribution: The working principle of this method [57] is that the difference between the pressures obtained from the measurement taps and the pressures derived from the pressure model is statistically different under normal and faulty situations. However, similar to the above, this method also has the disadvantage of being greatly affected by the variance of measurement noise. To fill the gap, the proposed algorithm is firstly applied to the fault detection of FADS.
4) For many laboratories and research institutions, it is costly and difficult to obtain the aerodynamic data through a large number of wind tunnel flight experiments. In this paper, CFX, a highly credible CFD software, is employed to acquire the data representing the numerical relationship between pressure values and the states such as α and β on the foundation of aerodynamics theory. Besides, FADS is an advanced sensor mounted on the hypersonic aircraft with an eye toward future aviation requirements, the working principle is analyzed in detail in this paper, which provides a reference for the follow-up research.
5) In order to demonstrate the effectiveness of the newly proposed method, a representative case is simulated digitally. Moreover, a further comparison with the two traditional methods and ordered weighted averaging (OWA) with different weight values is conducted under different noise conditions to prove the robustness and feasibility of the new method.
6) Overall, FADS system is a relatively new sensor used in hypersonic aircraft, and there are still some detailed knowledge that needs to be supplemented. The research in this paper enriches the theoretical knowledge of fault detection and provides a new solution for the problem of FADS, meanwhile, overcomes the drawbacks of previous methods.

The paper's structure is as follows: In Section 2, some related concepts are briefly reviewed. Moreover, a formula for calculating the similarity, as well as a score function, are proposed. In Section 3, an algorithm based on IVNSs, BRB and D-S evidence reasoning is derived. In Section 4, the aerodynamic model of FADS and an illustrative example concerning the fault detection are provided. In Section 5, the results obtained by the newly proposed method and other three methods are presented and compared. Finally, the conclusion of this paper is given in Section 6.

2. Related research on IVNSs, BRB, and D-S evidence reasoning

This paper provides a method for fault detection problem based on IVNSs, BRB, and D-S evidence reasoning. Here, we introduce some relevant concepts.

2.1. Preliminaries

Definition 1. A single-valued neutrosophic set, denoted as $A = \{\langle x, T_A(x), I_A(x), F_A(x)\rangle | x \in X\}$, where $X = \{x_1, x_2, \cdots, x_n\}$ represents a finite universe of discourse. $T_A(x)$, $I_A(x)$, and $F_A(x)$ denote the membership degree, uncertainty degree, and non-membership degree of an element x to A.

$$T_A(x) : X \rightarrow \ ]0^-, 1^+[$$
$$I_A(x) : X \rightarrow \ ]0^-, 1^+[$$
$$F_A(x) : X \rightarrow \ ]0^-, 1^+[$$

and

$$0^- \leq supT_A(x) + supI_A(x) + supF_A(x) \leq 3^+$$

Definition 2. Given a neutrosophic set $A = \{\langle x, T_A(x), I_A(x), F_A(x)\rangle | x \in X\}$, where $\left(T_A(x), I_A(x), F_A(x)\right) = \left([T_A^L(x),\ T_A^U(x)], [I_A^L(x),\ I_A^U(x)], [F_A^L(x),\ F_A^U(x)]\right)$, then, it is called the interval-valued neutrosophic sets (IVNSs).

$$T_A^L(x),\ T_A^U(x) : X \rightarrow \ ]0^-, 1^+[$$
$$I_A^L(x),\ I_A^U(x) : X \rightarrow \ ]0^-, 1^+[$$
$$F_A^L(x),\ F_A^U(x) : X \rightarrow \ ]0^-, 1^+[$$

Definition 3. Given two IVNSs A and B, if following conditions are satisfied, then A is called to be included in or equal to B, recorded as $A \subseteq B$.

$$infT_A(x) \geq infT_B(x),\ supT_A(x) \leq supT_B(x)$$
$$infI_A(x) \leq infI_B(x),\ supI_A(x) \geq supI_B(x)$$
$$infF_A(x) \leq infF_B(x),\ supF_A(x) \geq supF_B(x)$$

Definition 4. Let $\Theta = \{A_1, \cdots, A_n\}$ be the recognition frame. A basic probability assignment (BPA) is a function $m : 2^\Theta \rightarrow [0, 1]$, satisfying the following two formulas:

$$m(\varnothing) = 0 \tag{1}$$
$$\sum_{A \subseteq \Theta} m(A) = 1 \tag{2}$$

where $2^\Theta = \left\{\varnothing,\ \{\theta\}\right\}$ represents the power set of Θ; $\varnothing$ stands for the empty set.

Definition 5. Given a recognition frame Θ, the belief function $Bel(A)$ and plausibility function $Pl(A)$ based on BPA can be defined as:

$$Bel(A) = \sum_{B \subseteq A} m(B) \tag{3}$$
$$Pl(A) = \sum_{B \cap A \neq \varnothing} m(B) \tag{4}$$

Definition 6. Given two belief structures m_1 and m_2, the combinational rule $m_1 \oplus m_2(A)$ can be denoted as:

$$m_1 \oplus m_2(A) = \frac{1}{K} \sum_{B \cap C = A} m_1(B) m_2(C) \tag{5}$$

where $K = \sum_{B \cap C \neq \varnothing} m_1(B) m_2(C) = 1 - \sum_{B \cap C = \varnothing} m_1(B) m_2(C)$

Definition 7. Assume that there are n belief structures, the combinational rule is expressed as $m_1 \oplus m_2 \oplus \cdots \oplus m_n(A)$:

$$(m_1 \oplus m_2 \oplus \cdots \oplus m_n)(A) = \frac{1}{K} \sum_{A_1 \cap A_2 \cap \cdots \cap A_n = A} m_1(A_1) \cdots m_n(A_n) \tag{6}$$

where

$$K = \sum_{A_1 \cap A_2 \cap \cdots \cap A_n \neq \varnothing} m_1(A_1) m_2(A_2) \cdots m_n(A_n) = 1 - \sum_{A_1 \cap A_2 \cap \cdots \cap A_n = \varnothing} m_1(A_1) m_2(A_2) \cdots m_n(A_n)$$

Definition 8. Given a special case that two belief structures m_1 and m_2 are intervals, the combinational rule $m_1 \oplus m_2(A)$ can be denoted as:

$$\begin{aligned} &\max / \min \quad m_1 \oplus m_2(A) = \sum_{B \cap C = A} m_1(B) m_2(C) \\ &s.t. \quad \sum_{B \subseteq \Theta} m_1(B) = 1; \\ &\quad \sum_{C \subseteq \Theta} m_2(C) = 1; \\ &\quad inf\, m_1(B) \le m_1(B) \le sup m_1(B); \\ &\quad inf\, m_2(C) \le m_2(C) \le sup m_2(C). \end{aligned} \tag{7}$$

Definition 9. The belief rule base structure containing K rules can be described as:

$$IR = \langle (X,\ A),\ (Y,\ C),\ ICD,\ \Omega,\ W \rangle$$

Where $X = \{X_i | i = 1,\ 2,\ \cdots,\ I\}$ is the premise attribute set; $A = \{A(X_i) | i = 1,\ 2,\ \cdots,\ I\}$ stands for the attribute value set of X_i; $Y = \{Y_j | j = 1,\ 2,\ \cdots,\ J\}$ is the conclusion attribute set; $C = \{C(Y_j) | j = 1,\ 2,\ \cdots,\ J\}$ represents the attribute value set of Y_i; $ICD = \{Icd(\Psi) | Icd(\Psi) \in I_{[0,\,1]}\}$ is the belief set and $Icd(\Psi)$ evinces the belief degree of case Ψ; $\Omega = \{w^1,\ \cdots,\ w^k,\ \cdots,\ w^K\}$ represents the weight vector of rules and $0 \le w^k \le 1$; $W = \{w_1,\ \cdots,\ w_i,\ \cdots,\ w_I\}$ is the weight vector of premise attributes, $0 \le w_i \le 1$ and $\sum_{t=1}^{I} w_t = 1$.

Definition 10. The kth rule IR^k in BRB model $IR = \langle (X,\ A), (Y,\ C),\ ICD,\ \Omega,\ W \rangle$ means:
IF $\left(X_1 = A_1^k,\ Icd^k(X_1 = A_1^k)\right) \bigwedge \cdots \bigwedge \left(X_i = A_i^k,\ Icd^k(X_i = A_i^k)\right) \bigwedge \cdots \bigwedge \left(X_I = A_I^k,\ Icd^k(X_I = A_I^k)\right)$
THEN $\left(Y_1 = C_1^k,\ Icd^k(Y_1 = C_1^k)\right) \bigwedge \cdots \bigwedge \left(Y_j = C_j^k,\ Icd^k(Y_j = C_j^k)\right) \bigwedge \cdots \bigwedge \left(Y_J = C_J^k,\ Icd^k(Y_J = C_J^k)\right)$.
With $Icd^k(R^k)$, w^k, $W = \left\{w_1,\ \cdots, w_i, \cdots,\ w_I\right\}$
For short, the rule IR^k can be expressed as:
IF $\left(A_1^k,\ \alpha_1^k\right) \bigwedge \cdots \bigwedge \left(A_i^k,\ \alpha_i^k\right) \bigwedge \cdots \bigwedge \left(A_I^k,\ \alpha_I^k\right)$
THEN $\left(C_1^k,\ \beta_1^k\right) \bigwedge \cdots \bigwedge \left(C_j^k,\ \beta_j^k\right) \bigwedge \cdots \bigwedge \left(C_J^k,\ \beta_j^k\right)$.
With $Icd^k(R^k)$, w^k, $W = \left\{w_1,\ \cdots, w_i, \cdots,\ w_I\right\}$

Definition 11. The BRB model is:

$$IR = \langle (X,\ A),\ (Y,\ C),\ ICD,\ \Omega,\ W \rangle$$

and the input is

$$Input = \left\{\left(a_1,\ \alpha_1\right),\ \cdots,\ \left(a_i,\ \alpha_i\right),\ \cdots,\ \left(a_I,\ \alpha_I\right)\right\}$$

For any $i \in \left\{1,\ 2,\ \cdots,\ I\right\}$, if $A_i^k = a_i$ or $A_i^k = \phi$, the input $Input$ matches the rule IR^k and IR^k is activated successfully.

2.2. A new approach for calculating the similarity between different IVNSs

For the proposed method, how to calculate the similarity between IVNSs is a crucial step. First, we offer some previous studies.

Definition 12. Given two IVNSs $A = \{\langle x, ([T_A^L(x), T_A^U(x)], [I_A^L(x), I_A^U(x)], [F_A^L(x), F_A^U(x)]) \rangle | x \in X\}$ and $B = \{\langle x, ([T_B^L(x), T_B^U(x)], [I_B^L(x), I_B^U(x)], [F_B^L(x), F_B^U(x)]) \rangle | x \in X\}$.

a) Similarity measurement based on Hamming distance [58].

$$\begin{aligned} d_H(A, B) = \frac{1}{6}\big(&|T_A^L(x) - T_B^L(x)| + |T_A^U(x) - T_B^U(x)| + |I_A^L(x) - I_B^L(x)| + |I_A^U(x) - I_B^U(x)| + |F_A^L(x) - F_B^L(x)| + |F_A^U(x) - F_B^U(x)|\big); \\ &S_1(A, B) = 1 - d_H(A, B). \end{aligned} \tag{8}$$

b) Similarity measurement based on Euclidean distance [58].

$$\begin{aligned} d_E(A, B) = \Big[\frac{1}{6}\Big(&\left(T_A^L(x) - T_B^L(x)\right)^2 + \left(T_A^U(x) - T_B^U(x)\right)^2 + \left(I_A^L(x) - I_B^L(x)\right)^2 + \left(I_A^U(x) - I_B^U(x)\right)^2 \\ &+ \left(F_A^L(x) - F_B^L(x)\right)^2 + \left(F_A^U(x) - F_B^U(x)\right)^2\Big)\Big]^{\frac{1}{2}}; \\ &S_2(A, B) = 1 - d_E(A, B). \end{aligned} \tag{9}$$

c) Cosine similarity measurement [59].

$$S_3(A,B)=\frac{1}{2}\Big\{\big[T_A^L(x)T_B^L(x)+I_A^L(x)I_B^L(x)+F_A^L(x)F_B^L(x)+T_A^U(x)T_B^U(x)+I_A^U(x)I_B^U(x)+F_A^U(x)F_B^U(x)\big]/\\ \big[(T_A^L(x))^2+(I_A^L(x))^2+(F_A^L(x))^2+(T_A^U(x))^2+(I_A^U(x))^2+(F_A^U(x))^2\\ +(T_B^L(x))^2+(I_B^L(x))^2+(F_B^L(x))^2+(T_B^U(x))^2+(I_B^U(x))^2+(F_B^U(x))^2\big]\Big\} \tag{10}$$

Remark. Assume that $A_1=[0,\frac{1}{2}],[0,\frac{1}{2}],[0,0]$, $A_2=[0,0],[0,\frac{1}{2}],[0,\frac{1}{2}]$, and $B=[0,\frac{1}{2}],[0,\frac{1}{2}],[0,\frac{1}{2}]$, in terms of methods a) and b), the similarity values calculated by the two methods are equal, i.e., $S_1(A_1,B)=S_1(A_2,B)$ and $S_2(A_1,B)=S_2(A_2,B)$. However, it is obvious that the difference in non-membership between A_1 and B is the main cause for $S_1(A_1,B)$ and $S_2(A_1,B)$. On the contrary, $S_1(A_2,B)$ and $S_2(A_2,B)$ are obtained because of the inconsistency in membership. In other words, the two methods can only measure the similarity between IVNSs as a whole, but can not reveal the differences between sets in detail. For method c), it is worth noting that the results are always equal to 0 when $[T_A^L(x),T_A^U(x)]=[I_A^L(x),I_A^U(x)]=[F_A^L(x),F_A^U(x)]=[0,0]$ or $[T_B^L(x),T_B^U(x)]=[I_B^L(x),I_B^U(x)]=[F_B^L(x),F_B^U(x)]=[0,0]$, even the formula is meaningless if $A=B=[0,0],[0,0],[0,0]$, which suggests that there are still some limitations for the method.

Considering that it is flawed to make use of a single value to describe the similarity between IVNSs, meanwhile, in order to promote relevant research, we propose a new expression in this paper, i.e., interval-valued similarity. First, we will introduce four prerequisites that similarity must satisfy.

Theorem 1. *Suppose that A, B and C are three fuzzy sets, if $S(A,\ B)$ meets the following conditions, then it is called the similarity between A and B [60]:*

1) $0\le S(A,\ B)\le 1$;
2) *If $A=B$, then* $S(A,\ B)=1$;
3) $S(A,\ B)=S(B,\ A)$;
4) *If $A\subseteq B\subseteq C$, then* $S(A,\ C)\le S(A,\ B)$ *and* $S(A,\ C)\le S(B,\ C)$.

Definition 13. Given two IVNSs $A=\{\langle x,([T_A^L(x),T_A^U(x)],[I_A^L(x),I_A^U(x)],[F_A^L(x),F_A^U(x)])\rangle|x\in X\}$ and $B=\{\langle x,([T_B^L(x),T_B^U(x)],[I_B^L(x),I_B^U(x)],[F_B^L(x),F_B^U(x)])\rangle|x\in X\}$. The similarity $S(A,\ B)=([S_T^L(A,B),\ S_T^U(A,B)],\ [S_I^L(A,B),\ S_I^U(A,B)],\ [S_F^L(A,B),S_F^U(A,B)])$ between A and B is defined below.

$$S_T^L(A,B)=\min\Big\{\min\big\{1-T_A^L(x)+T_B^L(x),\ 1-T_B^L(x)+T_A^L(x)\big\},\ \min\big\{1-T_A^U(x)+T_B^U(x),1-T_B^U(x)+T_A^U(x)\big\}\Big\};$$

$$S_T^U(A,B)=\max\Big\{\min\big\{1-T_A^L(x)+T_B^L(x),1-T_B^L(x)+T_A^L(x)\big\},\ \min\big\{1-T_A^U(x)+T_B^U(x),1-T_B^U(x)+T_A^U(x)\big\}\Big\};$$

$$S_I^L(A,B)=\min\Big\{\min\big\{1-I_A^L(x)+I_B^L(x),1-I_B^L(x)+I_A^L(x)\big\},\ \min\big\{1-I_A^U(x)+I_B^U(x),1-I_B^U(x)+I_A^U(x)\big\}\Big\};$$

$$S_I^U(A,B)=\max\Big\{\min\big\{1-I_A^L(x)+I_B^L(x),1-I_B^L(x)+I_A^L(x)\big\},\ \min\big\{1-I_A^U(x)+I_B^U(x),1-I_B^U(x)+I_A^U(x)\big\}\Big\};$$

$$S_F^L(A,B)=\min\Big\{\min\big\{1-F_A^L(x)+F_B^L(x),1-F_B^L(x)+F_A^L(x)\big\},\ \min\big\{1-F_A^U(x)+F_B^U(x),1-F_B^U(x)+F_A^U(x)\big\}\Big\};$$

$$S_F^U(A,B)=\max\Big\{\min\big\{1-F_A^L(x)+F_B^L(x),1-F_B^L(x)+F_A^L(x)\big\},\ \min\big\{1-F_A^U(x)+F_B^U(x),1-F_B^U(x)+F_A^U(x)\big\}\Big\};$$

Proof 1. Given any three IVNSs $A=\{\langle x,T_A(x),I_A(x),F_A(x)\rangle|x\in X\}$, $B=\{\langle x,T_B(x),I_B(x),F_B(x)\rangle|x\in X\}$, and $C=\{\langle x,T_C(x),I_C(x),F_C(x)\rangle|x\in X\}$, where $(T_A(x),I_A(x),F_A(x))=([T_A^L(x),T_A^U(x)],[I_A^L(x),I_A^U(x)],[F_A^L(x),F_A^U(x)])$, $(T_B(x),I_B(x),F_B(x))=([T_B^L(x),T_B^U(x)],[I_B^L(x),I_B^U(x)],[F_B^L(x),F_B^U(x)])$, and $(T_C(x),I_C(x),F_C(x))=([T_C^L(x),T_C^U(x)],[I_C^L(x),I_C^U(x)],[F_C^L(x),F_C^U(x)])$, the proof process is as follows:

1) $0\le S(A,\ B)\le 1$.

Because

$$0\le T_A^L(x)\le 1,\quad 0\le T_A^U(x)\le 1;0\le I_A^L(x)\le 1,\quad 0\le I_A^U(x)\le 1;0\le F_A^L(x)\le 1,\quad 0\le F_A^U(x)\le 1;$$

and

$$0\le T_B^L(x)\le 1,\quad 0\le T_B^U(x)\le 1;0\le I_B^L(x)\le 1,\quad 0\le I_B^U(x)\le 1;0\le F_B^L(x)\le 1,\quad 0\le F_B^U(x)\le 1;$$

then

$$0\le\min\big\{1+T_A^L(x)-T_B^L(x),1-T_A^L(x)+T_B^L(x)\big\}\le 1,\quad 0\le\min\big\{1+T_A^U(x)-T_B^U(x),1-T_A^U(x)+T_B^U(x)\big\}\le 1;$$

therefore

$$0\le S_T^L(A,B)\le 1,\quad 0\le S_T^U(A,B)\le 1.$$

The other two cases are similar. So, we can obtain $S(A,B)\in[0,\ 1]$.

2) If $A=B$, then $S(A,\ B)=1$.

If

$$T_A^L(x) = T_B^L(x), \quad T_A^U(x) = T_B^U(x), I_A^L(x) = I_B^L(x), \quad I_A^U(x) = I_B^U(x), F_A^L(x) = F_B^L(x), \quad F_A^U(x) = F_B^U(x).$$

Then

$$\min\left\{\min\left\{1 - T_A^L(x) + T_B^L(x), 1 - T_B^L(x) + T_A^L(x)\right\}, \min\left\{1 - T_A^U(x) + T_B^U(x), 1 - T_B^U(x) + T_A^U(x)\right\}\right\} = 1;$$

$$\max\left\{\min\left\{1 - T_A^L(x) + T_B^L(x), 1 - T_B^L(x) + T_A^L(x)\right\}, \min\left\{1 - T_A^U(x) + T_B^U(x), 1 - T_B^U(x) + T_A^U(x)\right\}\right\} = 1;$$

$$\min\left\{\min\left\{1 - I_A^L(x) + I_B^L(x), 1 - I_B^L(x) + I_A^L(x)\right\}, \min\left\{1 - I_A^U(x) + I_B^U(x), 1 - I_B^U(x) + I_A^U(x)\right\}\right\} = 1;$$

$$\max\left\{\min\left\{1 - I_A^L(x) + I_B^L(x), 1 - I_B^L(x) + I_A^L(x)\right\}, \min\left\{1 - I_A^U(x) + I_B^U(x), 1 - I_B^U(x) + I_A^U(x)\right\}\right\} = 1;$$

$$\min\left\{\min\left\{1 - F_A^L(x) + F_B^L(x), 1 - F_B^L(x) + F_A^L(x)\right\}, \min\left\{1 - F_A^U(x) + F_B^U(x), 1 - F_B^U(x) + F_A^U(x)\right\}\right\} = 1;$$

$$\max\left\{\min\left\{1 - F_A^L(x) + F_B^L(x), 1 - F_B^L(x) + F_A^L(x)\right\}, \min\left\{1 - F_A^U(x) + F_B^U(x), 1 - F_B^U(x) + F_A^U(x)\right\}\right\} = 1.$$

3) $S(A,\ B) = S(B,\ A)$.

$$\begin{aligned}
S(A,\ B) &= \left([S_T^L(A,B),\ S_T^U(A,B)],\ [S_I^L(A,B),\ S_I^U(A,B)], [S_F^L(A,B),\ S_F^U(A,B)]\right) \\
&= \Big(\Big[\min\Big\{\min\left\{1 - T_A^L(x) + T_B^L(x),\ 1 - T_B^L(x) + T_A^L(x)\right\}, \min\left\{1 - T_A^U(x) + T_B^U(x),\ 1 - T_B^U(x) + T_A^U(x)\right\}\Big\}, \\
&\quad \max\Big\{\min\left\{1 - T_A^L(x) + T_B^L(x), 1 - T_B^L(x) + T_A^L(x)\right\}, \min\left\{1 - T_A^U(x) + T_B^U(x), 1 - T_B^U(x) + T_A^U(x)\right\}\Big\}\Big], \\
&\quad \Big[\min\Big\{\min\left\{1 - I_A^L(x) + I_B^L(x), 1 - I_B^L(x) + I_A^L(x)\right\}, \min\left\{1 - I_A^U(x) + I_B^U(x), 1 - I_B^U(x) + I_A^U(x)\right\}\Big\}, \\
&\quad \max\Big\{\min\left\{1 - I_A^L(x) + I_B^L(x), 1 - I_B^L(x) + I_A^L(x)\right\}, \min\left\{1 - I_A^U(x) + I_B^U(x), 1 - I_B^U(x) + I_A^U(x)\right\}\Big\}\Big]\Big) \\
&\quad \Big[\min\Big\{\min\left\{1 - F_A^L(x) + F_B^L(x), 1 - F_B^L(x) + F_A^L(x)\right\}, \min\left\{1 - F_A^U(x) + F_B^U(x), 1 - F_B^U(x) + F_A^U(x)\right\}\Big\}, \\
&\quad \max\Big\{\min\left\{1 - F_A^L(x) + F_B^L(x), 1 - F_B^L(x) + F_A^L(x)\right\}, \min\left\{1 - F_A^U(x) + F_B^U(x), 1 - F_B^U(x) + F_A^U(x)\right\}\Big\}\Big]\Big) \\
&= S(B,\ A).
\end{aligned}$$

4) If $A \subseteq B \subseteq C$, then $S(A,\ C) \leq S(A,\ B)$ and $S(A,\ C) \leq S(B,\ C)$.

If $A \subseteq B \subseteq C$, we can get following formulas according to *Definition 8*:

$$1 - T_A^L(x) + T_C^L(x) \leq 1 - T_C^L(x) + T_A^L(x); \quad 1 - T_A^L(x) + T_B^L(x) \leq 1 - T_B^L(x) + T_A^L(x).$$

Thus

$$\min\left\{1 - T_A^L(x) + T_C^L(x), 1 - T_C^L(x) + T_A^L(x)\right\} = 1 - T_A^L(x) + T_C^L(x);$$

and

$$\min\left\{1 - T_A^L(x) + T_B^L(x), 1 - T_B^L(x) + T_A^L(x)\right\} = 1 - T_A^L(x) + T_B^L(x).$$

Given that

$$T_C^L(x) \leq T_B^L(x)$$

therefore

$$1 - T_A^L(x) + T_C^L(x) \leq 1 - T_A^L(x) + T_B^L(x);$$

so

$$\min\left\{1 - T_A^L(x) + T_C^L(x), 1 - T_C^L(x) + T_A^L(x)\right\} \leq \min\left\{1 - T_A^L(x) + T_B^L(x), 1 - T_B^L(x) + T_A^L(x)\right\}.$$

Similar to the above, we can obtain:

$$S(A,\ C) \leq S(A,\ B),$$

and

$$S(A,\ C) \leq S(B,\ C).$$

Example 1. Given $A = \left([0.6,\ 0.7],\ [0.1,\ 0.2],\ [0.2,\ 0.25]\right)$ and $B = \left([0.4,\ 0.6],\ [0.2,\ 0.3],\ [0.5,\ 0.6]\right)$, then

a) $S_1(A,\ B) = 0.808$;
b) $S_2(A,\ B) = 0.783$;
c) $S_3(A,\ B) = 0.219$;
d) $S(A,\ B) = \left([0.8, 0.9],\ [0.9, 0.9],\ [0.65, 0.7]\right)$.

2.3. A new score function for quantifying the information contained in IVNSs

In addition to the above concepts, the score function of IVNSs that can compare the information contained in different sets also plays a vital role in the proposed method. However, limited by the universality of IVNSs, there have been few studies highlighting it. Here, we list some previous research results and propose our method on the basis of predecessors.

Definition 14. Given $A = \{\langle x,\ ([T_A^L(x),\ T_A^U(x)],\ [I_A^L(x),\ I_A^U(x)],\ [F_A^L(x),\ F_A^U(x)])\rangle | x \in X\}$:

a) Wang's score function S_W [61]:

$$S_W(A) = \frac{T_A^L(x) + T_A^U(x)}{2} + 1 - \frac{I_A^L(x) + I_A^U(x)}{2} + 1 - \frac{F_A^L(x) + F_A^U(x)}{2}. \tag{11}$$

Remark 1. It is easily seen, the final results are always equal to 2 as long as $T_A^L(x) + T_A^U(x) = I_A^L(x) + I_A^U(x) + F_A^L(x) + F_A^U(x)$, which is absolutely unreasonable. For instance, given two IVNSs $A = [0, 1], [0, 0], [0, 1]$ and $B = [0, 1], [0, 1], [0, 0]$, the equation $S_W(A) = S_W(B)$ can be obtained by (18). Nevertheless, difference between the two sets is quite obvious. In other words, the method still has room for improvement in distinguishing information contained in different IVNSs.

b) Tang's score function S_T [62]:

$$S_T(A) = \frac{1}{6}\Big(4 + T_A^L(x) + T_A^U(x) - I_A^L(x) - I_A^U(x) - F_A^L(x) - F_A^U(x)\Big). \tag{12}$$

Remark 2. Similar to a), the same shortcoming also exists in S_T when $T_A^L(x) + T_A^U(x) = I_A^L(x) + I_A^U(x) + F_A^L(x) + F_A^U(x)$.

c) Sahin's score function S_S [63]:

$$S_S(A) = \frac{1}{4}\Big(2 + T_A^L(x) + T_A^U(x) - 2I_A^L(x) - 2I_A^U(x) - F_A^L(x) - F_A^U(x)\Big). \tag{13}$$

Remark 3. There is a problem with the score function, i.e., information omission. The main reason is the insufficient use of the upper and lower bounds of the membership, uncertainty, and non-membership.

To avoid the shortcomings of above methods, a novel score function based on p-norm is proposed. Considering that SVNS is a special case of IVNSs; therefore, we will discuss the former for the sake of analysis.

Definition 15. Given a SVNS $A = \{\langle x,\ T_A(x),\ I_A(x),\ F_A(x)\rangle | x \in X\}$ and the reference SVNS $R = \{\langle x,\ 0,\ 0,\ 0\rangle | x \in X\}$, the p-norm distance of A from R taking into account the inherent fuzziness is $\big((T_A(x) - 0)^p + (I_A(x) - 0)^p + (F_A(x) - 0)^p + (1 - \pi_A(x))^p\big)^{1/p}$ and p-norm variation between membership and non-membership degree $\big|(T_A(x))^p - (F_A(x))^p\big|^{1/p}$, where $\pi_A(x)$ expresses the hesitancy degree of the set and can be calculated by $\pi_A(x) = 1 - T_A(x) - I_A(x) - F_A(x)$. The generalized knowledge measure of A is defined as:

$$K(A) = \frac{1}{2^{1/p} + 1}\Big[\big((T_A(x))^p + (I_A(x))^p + (F_A(x))^p + (1 - \pi_A(x))^p\big)^{1/p} + \big|(T_A(x))^p - (F_A(x))^p\big|^{1/p}\Big], \tag{14}$$

where $(p = 1,\ 2,\ \cdots)$.

The p-norm knowledge-based score function of A is:

$$J(A) = \left(\frac{e^{T_A(x) - F_A(x)} - 1}{e^{T_A(x) - F_A(x)} + 1}\right) K(A) \tag{15}$$

Extend the score function from SVNSs to IVNSs.

Definition 16. Given an IVNS $A = \{\langle x,\ ([T_A^L(x),\ T_A^U(x)],\ [I_A^L(x),\ I_A^U(x)],\ [F_A^L(x),\ F_A^U(x)])\rangle | x \in X\}$, the score function $J(A)$ can be presented as follows:

$$\begin{aligned} K(A) = \frac{1}{2^{1/p} + 1}\Bigg[\Bigg(\frac{1}{2}\Big(\big(T_A^L(x)\big)^p + \big(T_A^U(x)\big)^p + \big(I_A^L(x)\big)^p + \big(I_A^U(x)\big)^p + \big(F_A^L(x)\big)^p + \big(F_A^U(x)\big)^p\Big) + \frac{1}{2}\Big(\big(T_A^U(x) + I_A^U(x) \\ + F_A^U(x)\big)^p + \big(T_A^L(x) + I_A^L(x) + F_A^L(x)\big)^p\Big)\Bigg)^{1/p} + \left|\frac{1}{2}\Big(\big(T_A^U(x)\big)^p - \big(F_A^U(x)\big)^p + \big(T_A^L(x)\big)^p - \big(F_A^L(x)\big)^p\Big)\right|^{1/p}\Bigg]; \end{aligned} \tag{16}$$

$$J(A) = \left(\frac{e^{\frac{T_A^U(x) - F_A^U(x) + T_A^L(x) - F_A^L(x)}{2}} - 1}{e^{\frac{T_A^U(x) - F_A^U(x) + T_A^L(x) - F_A^L(x)}{2}} + 1}\right) K(A) \tag{17}$$

Example 2. Given $A = \big([0.6,\ 0.7],\ [0.1,\ 0.2],\ [0.2,\ 0.25]\big)$,

a) $S_W(A) = 2.275$;
b) $S_T(A) = 0.758$;
c) $S_S(A) = 0.563$;
d) when $p = 2$, $J(A) = 0.162$.

3. Algorithm progress

In this section, the inference process is given and the above concepts are applied to promote the proposed method.

Assume that the BRB model containing K rules is:

$$IR = \langle (X,\ A),\ (Y,\ C),\ ICD,\ \Omega,\ W \rangle$$

and the input is

$$Input = \{ (a_1,\ \alpha_1),\ \cdots,\ (a_i,\ \alpha_i),\ \cdots,\ (a_I,\ \alpha_I) \}$$

where $X = \{\alpha_i^k | i = 1, 2, \cdots, I,\ k = 1, 2, \cdots, K\}$ is the premise attribute set; $A = \{A(\alpha_i^k) | i = 1,\ 2,\ \cdots,\ I\}$ stands for the attribute value set of X_i; $Y = \{Y_j | j = 1,\ 2,\ \cdots,\ J\}$ is the conclusion attribute set; $C = \{C(Y_j) | j = 1,\ 2,\ \cdots,\ J\}$ represents the attribute value set of Y_i; $ICD = Icd^k(R^k) = \gamma^k \in I_{([0,\ 1],[0,\ 1],[0,\ 1])}$ evinces the certitude degree of R^k; $\Omega = \{w^1,\ \cdots,\ w^k,\ \cdots,\ w^K\}$ represents the weight vector of rules; $W = \{w_1^k,\ \cdots,\ w_i^k,\ \cdots,\ w_I^k\}$ is the weight vector of premise attributes in rule R^k. The main procedures of the developed method can be summarized as follows.

Step 1: Construct the BRB model.

Set a series of domains and calculate the proportions belonging to and not belonging to the domains respectively according to the distribution characteristics of measurement data.

Step 2: Determine if the input matches the rule IR^k.

If $A_i^k = a_i$ or $A_i^k = \phi$, the input $Input$ matches the rule IR^k, and IR^k is activated successfully.

Step 3: Calculate the similarity between IVNSs.

Use *Definition 13* to obtain the interval-valued similarity between the IVNSs of input and the IVNSs of premise attributes.

Step 4: Obtain the certitude degree $\tilde{\alpha}^k$ of attributes.

Because there is a case where premise attributes are empty sets, the weights belonging to attributes must be reset before calculation, and then obtain the activation weights $\tilde{w}_i^k$.

$$\tilde{w}_i^k = \frac{w_i^k}{\sum_{t=1}^{I} w_t^k}. \tag{18}$$

Then

$$\overline{w}_i^k = \frac{\tilde{w}_i^k}{\max\limits_{l=1,\cdots,I} \{\tilde{w}_l^k\}}. \tag{19}$$

Given the premise attributes are connected by logic "$\bigwedge$", the certitude degree of attributes can be synthesized according to T-norm operator [64]:

$$\tilde{\alpha}^k = \Big(\big[(\tilde{\alpha}^k)^{L_T}, (\tilde{\alpha}^k)^{U_T} \big], \big[(\tilde{\alpha}^k)^{L_I}, (\tilde{\alpha}^k)^{U_I} \big], \big[(\tilde{\alpha}^k)^{L_F}, (\tilde{\alpha}^k)^{U_F} \big] \Big),$$

where

$$(\tilde{\alpha}^k)^{L_T} = \prod_{i=1}^{I} \sqrt[I]{\big[(\tilde{\alpha}_i^k)^{L_T} \big]^{\overline{w}_i^k}};\ (\tilde{\alpha}^k)^{U_T} = \prod_{i=1}^{I} \sqrt[I]{\big[(\tilde{\alpha}_i^k)^{U_T} \big]^{\overline{w}_i^k}};$$

$$(\tilde{\alpha}^k)^{L_I} = \prod_{i=1}^{I} \sqrt[I]{\big[(\tilde{\alpha}_i^k)^{L_I} \big]^{\overline{w}_i^k}};\ (\tilde{\alpha}^k)^{U_I} = \prod_{i=1}^{I} \sqrt[I]{\big[(\tilde{\alpha}_i^k)^{U_I} \big]^{\overline{w}_i^k}};$$

$$(\tilde{\alpha}^k)^{L_F} = \prod_{i=1}^{I} \sqrt[I]{\big[(\tilde{\alpha}_i^k)^{L_F} \big]^{\overline{w}_i^k}};\ (\tilde{\alpha}^k)^{U_F} = \prod_{i=1}^{I} \sqrt[I]{\big[(\tilde{\alpha}_i^k)^{U_F} \big]^{\overline{w}_i^k}}.$$

Step 5: Calculate the activation weights w_A^k of each evidence and the activation weights w_{IR}^k of rules.

In BRB model, certitude degree of the rule IR^k that is expressed by γ^k and certitude degree of $\bigwedge A^k$ expressed by $\tilde{\alpha}^k$ make up the evidences of conclusions. The activation weights w_A^k of $\bigwedge A^k$ and the activation weights w_{IR}^k of IR^k are calculated as shown:

$$\begin{aligned} w_A^k &= \Big(\big[(w_A^k)^{L_T}, (w_A^k)^{U_T} \big], \big[(w_A^k)^{L_I}, (w_A^k)^{U_I} \big], \big[(w_A^k)^{L_F}, (w_A^k)^{U_F} \big] \Big) \\ &= \Big(\big[\frac{(\tilde{\alpha}^k)^{L_T}}{(\tilde{\alpha}^k)^{L_T} + (\gamma^k)^{U_T}},\ \frac{(\tilde{\alpha}^k)^{U_T}}{(\tilde{\alpha}^k)^{U_T} + (\gamma^k)^{L_T}} \big], \\ &\quad \big[\frac{(\tilde{\alpha}^k)^{L_I}}{(\tilde{\alpha}^k)^{L_I} + (\gamma^k)^{U_I}},\ \frac{(\tilde{\alpha}^k)^{U_I}}{(\tilde{\alpha}^k)^{U_I} + (\gamma^k)^{L_I}} \big], \\ &\quad \big[\frac{(\alpha^k)^{L_F}}{(\tilde{\alpha}^k)^{L_F} + (\gamma^k)^{U_F}},\ \frac{(\alpha^k)^{U_F}}{(\tilde{\alpha}^k)^{U_F} + (\gamma^k)^{L_F}} \big] \Big), \end{aligned}$$

and

$$w_{IR}^k = \Big(\big[(w_{IR}^k)^{L_T}, (w_{IR}^k)^{U_T}\big], \big[(w_{IR}^k)^{L_I}, (w_{IR}^k)^{U_I}\big], \big[(w_{IR}^k)^{L_F}, (w_{IR}^k)^{U_F}\big]\Big)$$
$$= \Big(\big[\frac{(\gamma^k)^{L_T}}{(\tilde{\alpha}^k)^{U_T} + (\gamma^k)^{L_T}}, \frac{(\gamma^k)^{U_T}}{(\tilde{\alpha}^k)^{L_T} + (\gamma^k)^{U_T}}\big], \big[\frac{(\gamma^k)^{L_I}}{(\tilde{\alpha}^k)^{U_I} + (\gamma^k)^{L_I}}, \frac{(\gamma^k)^{U_I}}{(\tilde{\alpha}^k)^{L_I} + (\gamma^k)^{U_I}}\big], \big[\frac{(\gamma^k)^{L_F}}{(\tilde{\alpha}^k)^{U_F} + (\gamma^k)^{L_F}}, \frac{(\gamma^k)^{U_F}}{(\tilde{\alpha}^k)^{L_F} + (\gamma^k)^{U_F}}\big]\Big).$$

Step 6: Obtain the certitude degree $\tilde{\beta}^k$ of conclusions $\wedge C^k$.

Basic assignment functions are:

$$m_{\Theta^k}\big((\wedge A^k, \tilde{\alpha}^k)\big) = w_A^k \tilde{\alpha}^k;$$
$$m_{2^{\Theta^k}}\big((\wedge A^k, \tilde{\alpha}^k)\big) = 1 - w_A^k \tilde{\alpha}^k;$$
$$\overline{m}_{2^{\Theta^k}}\big((\wedge A^k, \tilde{\alpha}^k)\big) = 1 - w_A^k,$$

where $m_{\Theta^k}\big((\wedge A^k, \tilde{\alpha}^k)\big)$ stands for the certainty degree that is assigned to conclusions $\wedge C^k$ caused by $\wedge A^k$; $m_{2^{\Theta^k}}\big((\wedge A^k, \tilde{\alpha}^k)\big)$ represents the certainty degree that is not assigned to conclusions $\wedge C^k$ caused by $\wedge A^k$; $\overline{m}_{2^{\Theta^k}}\big((\wedge A^k, \tilde{\alpha}^k)\big)$ is the certainty degree that is not assigned to conclusions $\wedge C^k$ caused by the activation weights of $\wedge A^k$.

$$m_{\Theta^k}\big((IR^k, \gamma^k)\big) = w_{IR}^k \gamma^k;$$
$$m_{2^{\Theta^k}}\big((IR^k, \gamma^k)\big) = 1 - w_{IR}^k \gamma^k;$$
$$\overline{m}_{2^{\Theta^k}}\big((IR^k, \gamma^k)\big) = 1 - w_{IR}^k,$$

where $m_{\Theta^k}\big((IR^k, \gamma^k)\big)$ stands for the certainty degree that is assigned to conclusions $\wedge C^k$ caused by IR^k; $m_{2^{\Theta^k}}\big((IR^k, \gamma^k)\big)$ represents the certainty degree that is not assigned to conclusions $\wedge C^k$ caused by IR^k; $\overline{m}_{2^{\Theta^k}}\big((IR^k, \gamma^k)\big)$ is the certainty degree that is not assigned to conclusions $\wedge C^k$ caused by the activation weights of IR^k.

Then, synthesize the uncertainty of evidences and acquire the synthetic basic probability assignment m_{Θ^k} and $\overline{m}_{2^{\Theta^k}}$.

$$m_{\Theta^k} = m_{\Theta^k}\big((IR^k, \gamma^k)\big) m_{\Theta^k}\big((\wedge A^k, \tilde{\alpha}^k)\big) + m_{\Theta^k}\big((IR^k, \gamma^k)\big) m_{2^{\Theta^k}}\big((\wedge A^k, \tilde{\alpha}^k)\big) + m_{2^{\Theta^k}}^{U_T}\big((IR^k, \gamma^k)\big) m_{\Theta^k}\big((\wedge A^k, \tilde{\alpha}^k)\big);$$

and

$$\overline{m}_{2^{\Theta^k}} = \overline{m}_{2^{\Theta^k}}\big((IR^k, \gamma^k)\big) m_{2^{\Theta^k}}\big((\wedge A^k, \tilde{\alpha}^k)\big).$$

The certitude degree $\tilde{\beta}^k$ of conclusions $\wedge C^k$ can be obtained:

$$\tilde{\beta}^k = \Big(\big[(\tilde{\beta}^k)^{L_T}, (\tilde{\beta}^k)^{U_T}\big], \big[(\tilde{\beta}^k)^{L_I}, (\tilde{\beta}^k)^{U_I}\big], \big[(\tilde{\beta}^k)^{L_F}, (\tilde{\beta}^k)^{U_F}\big]\Big)$$
$$= \Big(\min\Big\{\frac{m_{\Theta^k}^T}{1 - \overline{m}_{2^{\Theta^k}}^T}, 1\Big\}, \min\Big\{\frac{m_{\Theta^k}^I}{1 - \overline{m}_{2^{\Theta^k}}^I}, 1\Big\}, \min\Big\{\frac{m_{\Theta^k}^F}{1 - \overline{m}_{2^{\Theta^k}}^F}, 1\Big\}\Big)$$

Step 7: Obtain the certitude degree of conclusion attributes under the input condition $\tilde{\beta}_j^k$.

Utilize the similarity method and certitude degree of each conclusion in the rule, obtain the certitude degree of conclusions under the input fact condition.

$$\tilde{\beta}_j^k = \Big(\big[(\tilde{\beta}_j^k)^{L_T}, (\tilde{\beta}_j^k)^{U_T}\big], \big[(\tilde{\beta}_j^k)^{L_I}, (\tilde{\beta}_j^k)^{U_I}\big], \big[(\tilde{\beta}_j^k)^{L_F}, (\tilde{\beta}_j^k)^{U_F}\big]\Big);$$

where

$$(\tilde{\beta}_j^k)^{L_T} = \min\Big\{(\tilde{\tilde{\beta}}_j^k)^{L_T}(\beta_j^k)^{L_T}, 1\Big\}; (\tilde{\beta}_j^k)^{U_T} = \min\Big\{(\tilde{\tilde{\beta}}_j^k)^{U_T}(\beta_j^k)^{U_T}, 1\Big\};$$
$$(\tilde{\beta}_j^k)^{L_I} = \min\Big\{(\tilde{\tilde{\beta}}_j^k)^{L_I}(\beta_j^k)^{L_I}, 1\Big\}; (\tilde{\beta}_j^k)^{U_I} = \min\Big\{(\tilde{\tilde{\beta}}_j^k)^{U_I}(\beta_j^k)^{U_I}, 1\Big\};$$
$$(\tilde{\beta}_j^k)^{L_F} = \min\Big\{(\tilde{\tilde{\beta}}_j^k)^{L_F}(\beta_j^k)^{L_F}, 1\Big\}; (\tilde{\beta}_j^k)^{U_F} = \min\Big\{(\tilde{\tilde{\beta}}_j^k)^{U_F}(\beta_j^k)^{U_F}, 1\Big\}$$

and

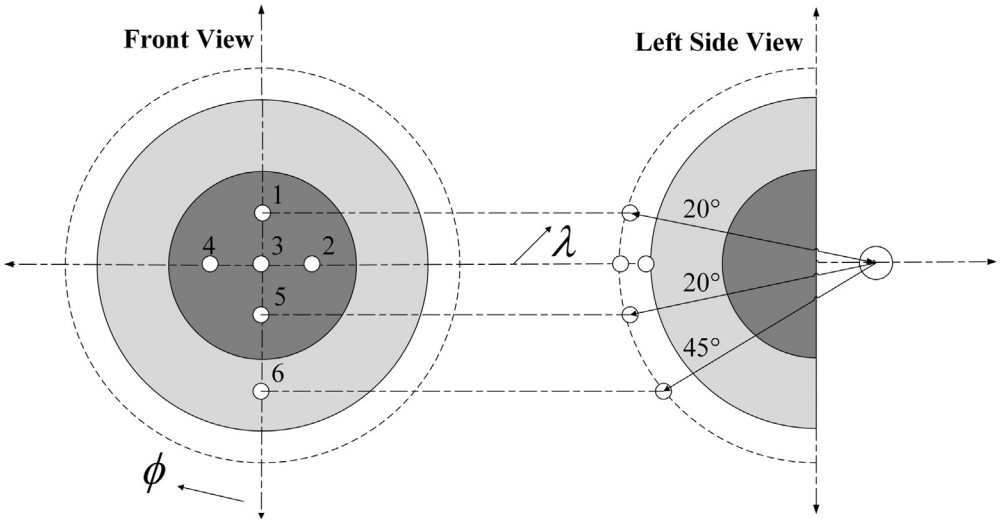

Fig. 1. Position of each measurement tap in FADS system.

$$(\tilde{\beta}_j^k)^{L_T} = \min\left\{1-(\beta_j^k)^{L_T}+(\tilde{\beta}^k)^{L_T}, 1-(\beta_j^k)^{U_T}+(\tilde{\beta}^k)^{U_T}\right\}; (\tilde{\beta}_j^k)^{U_T} = \max\left\{1-(\beta_j^k)^{L_T}+(\tilde{\beta}^k)^{L_T}, 1-(\beta_j^k)^{U_T}+(\tilde{\beta}^k)^{U_T}\right\};$$
$$(\tilde{\beta}_j^k)^{L_I} = \min\left\{1-(\beta_j^k)^{L_I}+(\tilde{\beta}^k)^{L_I}, 1-(\beta_j^k)^{U_I}+(\tilde{\beta}^k)^{U_I}\right\}; (\tilde{\beta}_j^k)^{U_I} = \max\left\{1-(\beta_j^k)^{L_I}+(\tilde{\beta}^k)^{L_I}, 1-(\beta_j^k)^{U_I}+(\tilde{\beta}^k)^{U_I}\right\}.$$
$$(\tilde{\beta}_j^k)^{L_F} = \min\left\{1-(\beta_j^k)^{L_F}+(\tilde{\beta}^k)^{L_F}, 1-(\beta_j^k)^{U_F}+(\tilde{\beta}^k)^{U_F}\right\}; (\tilde{\beta}_j^k)^{U_F} = \max\left\{1-(\beta_j^k)^{L_F}+(\tilde{\beta}^k)^{L_F}, 1-(\beta_j^k)^{U_F}+(\tilde{\beta}^k)^{U_F}\right\};$$

Step 8: Rank all of the alternatives.

Utilize the score function proposed in *Definition 15* to rank all alternatives, and then, regard the conclusion with the highest score as the final result.

4. Application in flush air data sensing

During flight process, the measurement results of airborne sensors play an important role in mastering the flight state. So, whether the measurement data of sensors is correct or not will directly affect the safety of the whole flight. Among the numerous sensors, atmospheric data sensor is undoubtedly a significant part that cannot be ignored. Traditionally, probe air data sensor is on the basis of pitot tube, the sensor measuring angle of attack α, and the sensor measuring angle of sideslip β. Given that the flight envelope of modern aircraft is getting larger, the complicated flight environment is prone to causing the damage of probe air data sensor, meanwhile, the exposed probe is not suitable for the modern aircraft pursuing the stealth effect. Therefore, flush air data sensing (FADS), an advanced and potential airborne sensor, is a good substitute. Different from the traditional air data sensor, FADS is dedicated to making use of the pressure sensors embedded in the body to derive α and β, which can effectively overcome the shortcomings of the traditional probe sensor [65,66]. By the way, it is because of the failure of the traditional sensor measuring α, two tragic air crash incidents of PT Lion Mentari Airlines and Ethiopian Airlines occurred in 2018 and 2019, resulting in 346 deaths. Therefore, the fault detection of FADS is of great significance to ensure the whole flight safety.

4.1. Aerodynamic model of FADS

The aerodynamic model of the FADS system combines the potential flow model (under subsonic conditions) and the modified Newtonian model (under supersonic conditions) with a correction coefficient ε to meet the requirements applicable in a large Mach range. In the subsonic case, the function can be calculated as the isentropic flow; On the contrary, the function can be obtained from the adiabatic positive shock relation in the supersonic case. The pressure for any surface tap $p(\theta)$ can be expressed as:

$$p(\theta) = q_c[\cos^2(\theta) + \varepsilon \sin^2(\theta)] + P_\infty \tag{20}$$

where q_c and P_∞ represent the dynamic pressure and static pressure; the shaped pressure coefficient ε is affected simultaneously by α, β, and the flight Mach M_∞, recorded as $\varepsilon = f(\alpha, \beta, M_\infty)$. The airflow incidence angle θ is defined as the angle between the surface normal direction and flow velocity vector direction for any surface tap, given as:

$$\cos(\theta) = \cos(\alpha)\cos(\beta)\cos(\lambda) + \sin(\beta)\sin(\phi)\sin(\lambda) + \sin(\alpha)\cos(\beta)\cos(\phi)\sin(\lambda) \tag{21}$$

where ϕ and λ indicate the circumferential angle and cone angle of each measurement tap, respectively. The position of each measurement tap refers to the system in X-33 aircraft, as shown in Fig. 1, Table 1 expresses the values of ϕ and λ.

For (20), according to the isentropic flow method and Rayleigh Pitot tube formula, the relation between M_∞, q_c, and P_∞ is approximately determined by

Table 1
The circumferential angle and cone angle of each measurement tap.

The number of measurement tap	The circumferential angle ϕ	The cone angle λ
1	180°	20°
2	270°	20°
3	0	0
4	90°	20°
5	0	20°
6	0	45°

$$\frac{q_c}{P_\infty} = \begin{cases} (1.0 + 0.2M_\infty^2)^{3.5} - 1, & (M_\infty \le 1) \\ 166.92M_\infty^2 (\frac{M_\infty^2}{7M_\infty^2 - 1})^{2.5} - 1, & (M_\infty > 1) \end{cases} \tag{22}$$

For the system, the method of measuring α is called three-point method, i.e., utilize three of the four taps numbered 1, 3, 5 and 6 in the longitudinal distribution to obtain α. The reason for not adopting tap 2 and tap 4 is that when α changes, the pressure values of the two horizontally distributed taps will not change much. In other words, it does not reflect the change of α very well, which will inevitably affect the measurement accuracy.

By combining (20) $\sim$ (22), the formula for calculating α is expressed as:

$$\alpha = \begin{cases} \frac{1}{2}\tan^{-1}(\frac{A}{B}), & |\alpha| \le 45° \\ \frac{1}{2}(\pi - \tan^{-1}(\frac{A}{B})), & |\alpha| > 45° \end{cases} \tag{23}$$

where

$$\begin{aligned} A &= \Gamma_{ik}\sin^2\lambda_j + \Gamma_{ji}\sin^2\lambda_k + \Gamma_{kj}\sin^2\lambda_i \\ B &= \Gamma_{ik}\cos\phi_j \sin\lambda_j \cos\lambda_j + \Gamma_{ji}\cos\phi_k \sin\lambda_k \cos\lambda_k + \Gamma_{kj}\cos\phi_i \sin\lambda_i \cos\lambda_i \end{aligned} \tag{24}$$

and

$$\Gamma_{ik} = p_i - p_k, \quad \Gamma_{ji} = p_j - p_i, \quad \Gamma_{kj} = p_k - p_j. \tag{25}$$

Obviously, there are $C_4^3 = 4$ combinations to obtain α, namely α_1 obtained from the combination of taps (1,3,5), α_2 obtained from the combination of taps (1,3,6), α_3 obtained from the combination of taps (1,5,6), and α_4 obtained from the combination of taps (3,5,6). The final output is defined as:

$$\alpha = \frac{\alpha_1 + \alpha_2 + \alpha_3 + \alpha_4}{4} \tag{26}$$

For driving the model with interpolation table, high precision aerodynamic data representing the numerical relationship between the pressure values of taps and α, M_∞, altitude H is acquired by the software CFX, as shown in Fig. 2 and Fig. 3. Here, some typical state points are listed as an example.

4.2. Fault scenarios

Compared with the traditional probe air data sensor, FADS possesses great advantages in measurement accuracy and reliability. Nevertheless, considering that it is mainly used in hypersonic aircraft such as X-33, complex flight environment and high body surface temperature may cause the system failure. Usually, the fault scenarios of FADS can be divided into two types: external factors and internal factors. The former mainly indicates that the special air flow environment leads to the damage of measurement taps, while the latter mainly includes tube leakage, electromagnetic interference, and circuit damage. In terms of FADS, the external factors occupy the main part due to the specific application scenarios. Therefore, suppose that when FADS fails, some measurement taps are damaged.

4.3. Illustrative example

The method introduced in Section 3 should be put into practice. Suppose that the BRB model contains five rules, denoted by IR^1 (tap 1 faults), IR^2 (tap 5 faults), IR^3 (taps 1 and 6 fault), IR^4 (taps 3 and 5 fault), and IR^5 (all normal). Measurement results of α_1, α_2, α_3, and α_4 consist of the premise attributes; we set the weight vector of the attributes $W = \{w_1, w_2, w_3, w_4\} = \{0.3, 0.2, 0.2, 0.3\}$ to express the difference. Similar to it, conclusions are also given in the form of IVNSs. Given that the importance of each rule is different, the weight vector $\Omega = \{w^1, w^2, w^3, w^4, w^5\}$ is adopted, γ^k represents the certitude degree of kth rule. Assume that the actual α is $-3°$. It is worth mentioning that in order to simulate the working environment of this sensor, we have added many noise interferences to the model, not just the measurement taps. Due to the failure of tap 1, the four sets of measurements α_1, α_2, α_3, and α_4 under various interference noises are abnormal, as shown in Fig. 4. In order to derive IVNSs, we set the domains $a_{-2} = [-6, -4]$, $a_{-1} = [-4, -2]$, $a_0 = [-2, 0]$, $a_1 = [0, 2]$, $a_2 = [2, 4]$, $a_3 = [4, 6]$.

The procedures for detecting the fault are summarized in the following steps.

Step 1: Construct the BRB model.

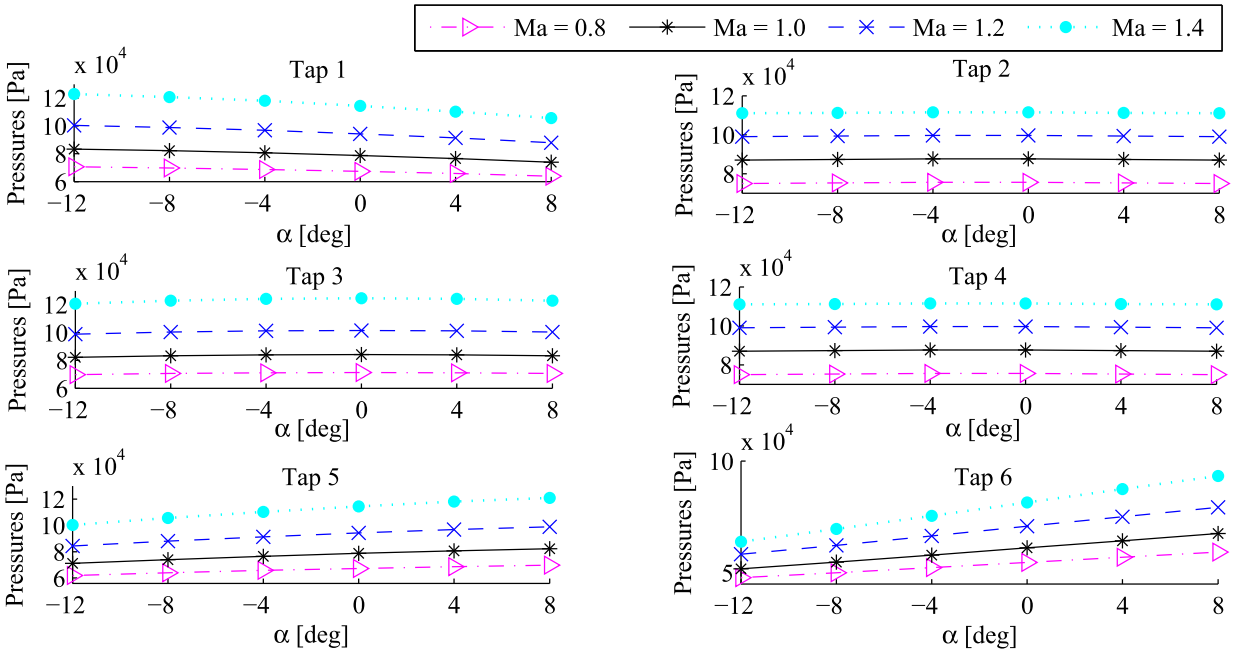

Fig. 2. Aerodynamic data when H = 10000 m.

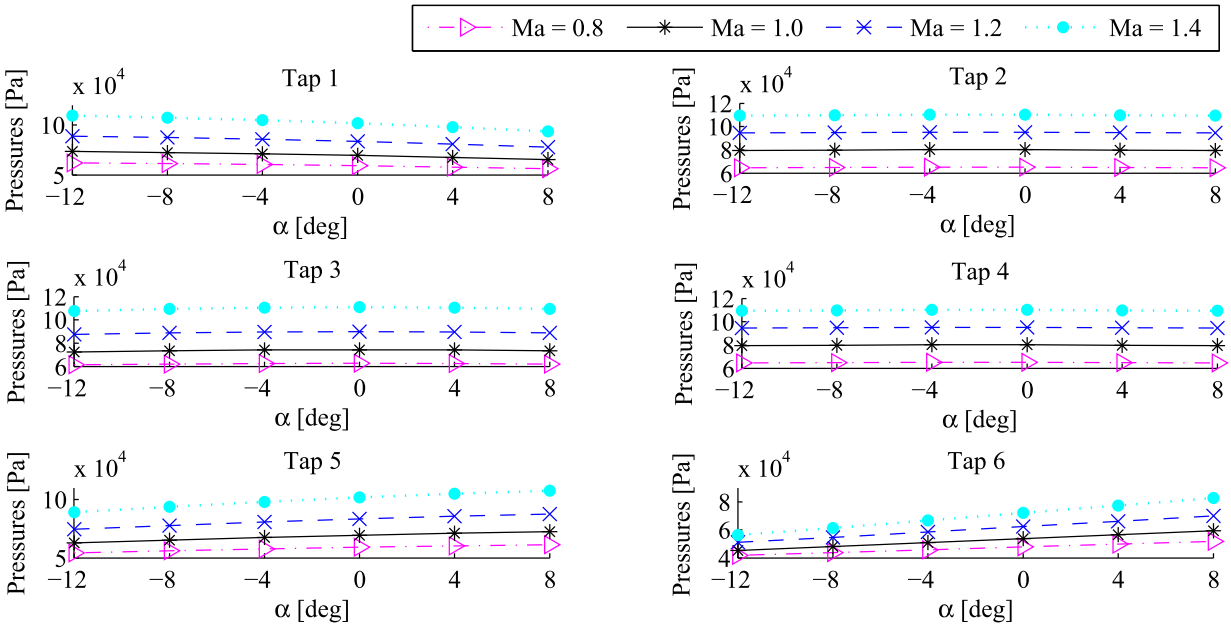

Fig. 3. Aerodynamic data when H = 12000 m.

According to Fig. 4, the membership, non-membership, and uncertainty degree in the IVNS of input can be obtained with the proportions belonging to and not belonging to the domain. The points which are exactly equal to the upper and lower bounds of domain are regarded as the uncertain points and the proportion is the uncertainty degree of IVNS. To emphasize the uncertainty and randomness, the three proportions will be reasonably expanded into the interval form. In this way, $Input = \{(a_0, [0.5, 0.62], [0.2, 0.25], [0.1, 0.15]), (a_{-1}, [0.6, 0.7], [0.04, 0.1], [0.2, 0.35]), (a_2, [0.8, 0.82], [0.1, 0.13], [0.05, 0.08]), (a_{-1}, [0.6, 0.65], [0.3, 0.32], [0.1, 0.13])\}$. The premise attributes in the form of IVNSs can also be acquired in the same way. Results are shown in Table 2. The values of $\wedge C^k$, w^k, and γ^k are offered by experts and engineering experience.

Step 2: Determine if the input matches the rule IR^k.

Obviously, the input matches IR^1, IR^3, and IR^4 because of the consistency on premise attributes.

Step 3: Calculate the similarity between IVNSs.

The similarity between input and attributes are gained with the proposed approach in *Definition 13*, as shown in Table 3.

Step 4: Obtain the certitude degree $\tilde{\alpha}^k$ of attributes.

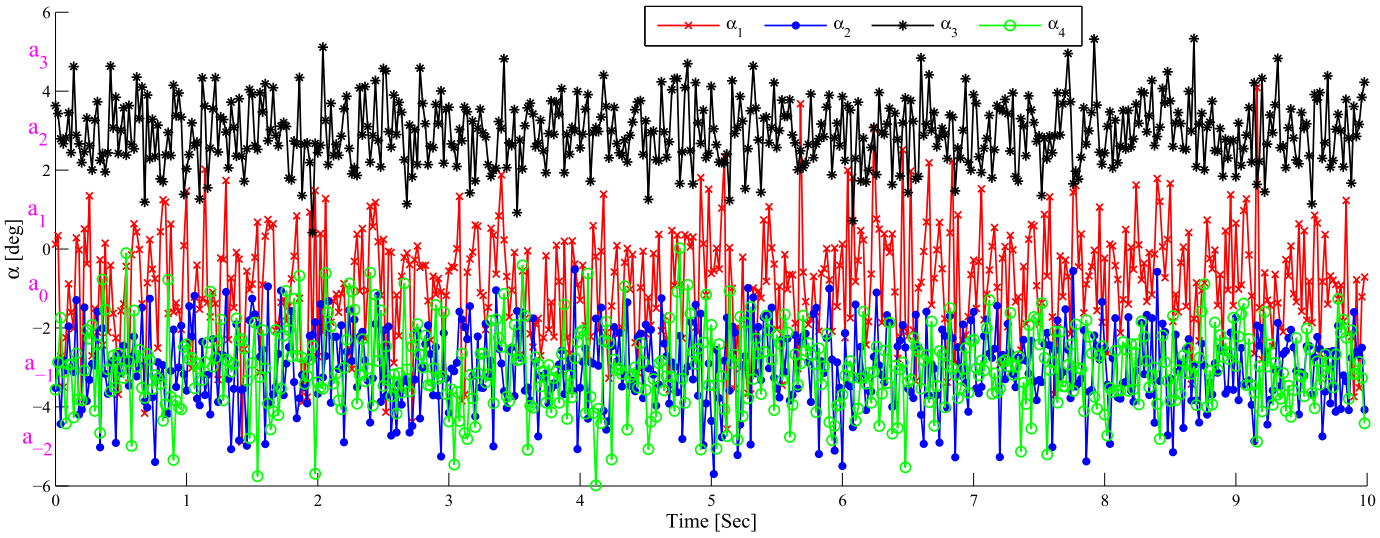

Fig. 4. Measurement results when tap 1 faults.

Table 2
BRB model in the form of IVNSs.

Rule IR^k	Premise $\wedge A^k$	Weights w^k
IR^1	$(a_0, [0.6, 0.63], [0.2, 0.35], [0.1, 0.2]) \wedge (a_{-1}, [0.5, 0.56], [0.13, 0.2], [0.2, 0.3])$ $\wedge(a_2, [0.4, 0.5], [0.24, 0.3], [0.2, 0.38]) \wedge (a_{-1}, [0.6, 0.63], [0.23, 0.4], [0.12, 0.13])$	0.7
IR^2	$(a_{-2}, [0.89, 0.92], [0.03, 0.05], [0.1, 0.15]) \wedge (a_0, [0.8, 0.9], [0.07, 0.08], [0.1, 0.15])$ $\wedge(a_{-1}, [0.8, 0.87], [0.02, 0.1], [0.11, 0.15]) \wedge (a_0, [0.7, 0.9], [0.1, 0.2], [0.09, 0.12])$	0.9
IR^3	$(a_0, [0.89, 0.93], [0, 0.07], [0.12, 0.13]) \wedge (a_{-1}, [0.61, 0.71], [0.25, 0.35], [0.3, 0.35])$ $\wedge(a_2, [0.61, 0.66], [0.34, 0.45], [0.08, 0.14]) \wedge (a_{-1}, [0.83, 0.92], [0.1, 0.14], [0.3, 0.45])$	0.8
IR^4	$(a_0, [0.62, 0.72], [0.12, 0.23], [0.1, 0.15]) \wedge (a_{-1}, [0.78, 0.84], [0.13, 0.18], [0.2, 0.3])$ $\wedge(a_2, [0.64, 0.7], [0.12, 0.23], [0.12, 0.2]) \wedge (a_{-1}, [0.78, 0.95], [0.05, 0.09], [0.08, 0.1])$	0.8
IR^5	$(a_{-1}, [0.7, 0.74], [0.1, 0.15], [0.1, 0.14]) \wedge (a_{-1}, [0.6, 0.65], [0.3, 0.32], [0.1, 0.13])$ $\wedge(a_{-1}, [0.74, 0.78], [0.04, 0.06], [0.13, 0.15]) \wedge (a_{-1}, [0.84, 0.89], [0.01, 0.02], [0.09, 0.1])$	0.8
Rule IR^k	Conclusion $\wedge C^k$	Belief degree γ^k
IR^1	$(c^1, [0.78, 0.9], [0.05, 0.12], [0.03, 0.1])$	$([0.78, 0.79], [0.11, 0.2], [0.08, 0.12])$
IR^2	$(c^2, [0.8, 0.91], [0.06, 0.13], [0.2, 0.3])$	$([0.78, 0.9], [0.1, 0.2], [0.2, 0.35])$
IR^3	$(c^3, [0.82, 0.9], [0.15, 0.2], [0.13, 0.15])$	$([0.72, 0.8], [0.01, 0.1], [0.2, 0.3])$
IR^4	$(c^4, [0.8, 0.87], [0.05, 0.09], [0.07, 0.11])$	$([0.85, 0.9], [0.25, 0.31], [0.03, 0.1])$
IR^5	$(c^5, [0.91, 0.94], [0.02, 0.04], [0.03, 0.06])$	$([0.74, 0.81], [0.1, 0.12], [0.09, 0.1])$

Table 3
Similarity between Input and Premise Attributes.

Rule IR^k	a_0	a_{-1}	a_2	a_{-1}
IR^1	[0.9,0.99],[0.8,0.9],[0.9,0.95]	[0.86,0.9],[0.85,0.93],[0.8,0.84]	[0.6,0.68],[0.78,0.81],[0.75,0.9]	[0.98,1],[0.73,0.87],[0.81,0.82]
IR^3	[0.61,0.69],[0.9,0.92],[0.88,0.92]	[0.99,0.99],[0.95,1],[0.74,0.75]	[0.81,0.84],[0.63,0.71],[0.98,0.99]	[0.73,0.77],[0.99,1],[0.87,1]
IR^4	[0.88,0.9],[0.92,0.98],[0.9,0.9]	[0.82,0.86],[0.83,0.93],[0.8,0.84]	[0.84,0.88],[0.85,0.93],[0.93,0.98]	[0.7,0.82],[0.95,0.96],[0.78,0.78]

IR^1:

$$\tilde{\alpha}^1 = [0.868, 0.919], [0.816, 0.897], [0.849, 0.897];$$

IR^3:

$$\tilde{\alpha}^3 = [0.787, 0.828], [0.892, 0.925], [0.887, 0.932];$$

IR^4:

$$\tilde{\alpha}^4 = [0.833, 0.885], [0.912, 0.961], [0.871, 0.886].$$

Step 5: Calculate the activation weights w_A^k of each evidence and the activation weights w_{IR}^k of rules.

Table 4
Rankings with different p.

Rule IR^k	IR^1	IR^3	IR^4	Ranking
p = 1	0.399	0.375	0.386	$c^1 > c^4 > c^3$
p = 2	0.381	0.345	0.369	$c^1 > c^4 > c^3$
p = 5	0.393	0.357	0.376	$c^1 > c^4 > c^3$
p = 8	0.405	0.368	0.384	$c^1 > c^4 > c^3$
p = 10	0.411	0.374	0.389	$c^1 > c^4 > c^3$

IR^1:

$$w_A^1 = [0.524, 0.541], [0.803, 0.891], [0.876, 0.918];$$

$$w_{IR}^1 = [0.459, 0.477], [0.109, 0.197], [0.082, 0.124].$$

IR^3:

$$w_A^3 = [0.496, 0.535], [0.899, 0.989], [0.747, 0.823];$$

$$w_{IR}^3 = [0.465, 0.504], [0.011, 0.101], [0.177, 0.253].$$

IR^4:

$$w_A^4 = [0.481, 0.510], [0.746, 0.794], [0.897, 0.967];$$

$$w_{IR}^4 = [0.490, 0.520], [0.206, 0.254], [0.033, 0.103].$$

Step 6: Obtain the certitude degree $\tilde{\beta}^k$ of conclusions $\wedge C^k$.

IR^1:

$$\tilde{\beta}^1 = [0.882, 0.974], [0.787, 1], [0.882, 1];$$

IR^3:

$$\tilde{\beta}^3 = [0.822, 0.990], [0.868, 1], [0.816, 1];$$

IR^4:

$$\tilde{\beta}^4 = [0.883, 1], [0.847, 1], [0.897, 1].$$

Step 7: Obtain the certitude degree of conclusion attributes under the input condition $\tilde{\beta}_j^k$.

IR^1:

$$\tilde{\beta}_j^1 = [0.838, 0.992], [0.087, 0.226], [0.056, 0.190];$$

IR^3:

$$\tilde{\beta}_j^3 = [0.822, 0.981], [0.258, 0.360], [0.219, 0.278];$$

IR^4:

$$\tilde{\beta}_j^4 = [0.866, 0.983], [0.090, 0.172], [0.128, 0.208].$$

Step 8: Rank all of the alternatives.

The final results calculated by the new score function are shown in Table 4. No matter what the values of p are, the final ranking is always $c^1 > c^4 > c^3$. Thus, the conclusion is that tap 1 faults.

5. Comparative analysis and discussion

In order to illustrate the rationality of the proposed method, a comparison is going to be performed with other three methods, including the methods with parity equation [56], χ^2 distribution [57], and ordered weighted averaging (OWA) [67]. The comparison analysis is based on the same illustrative example.

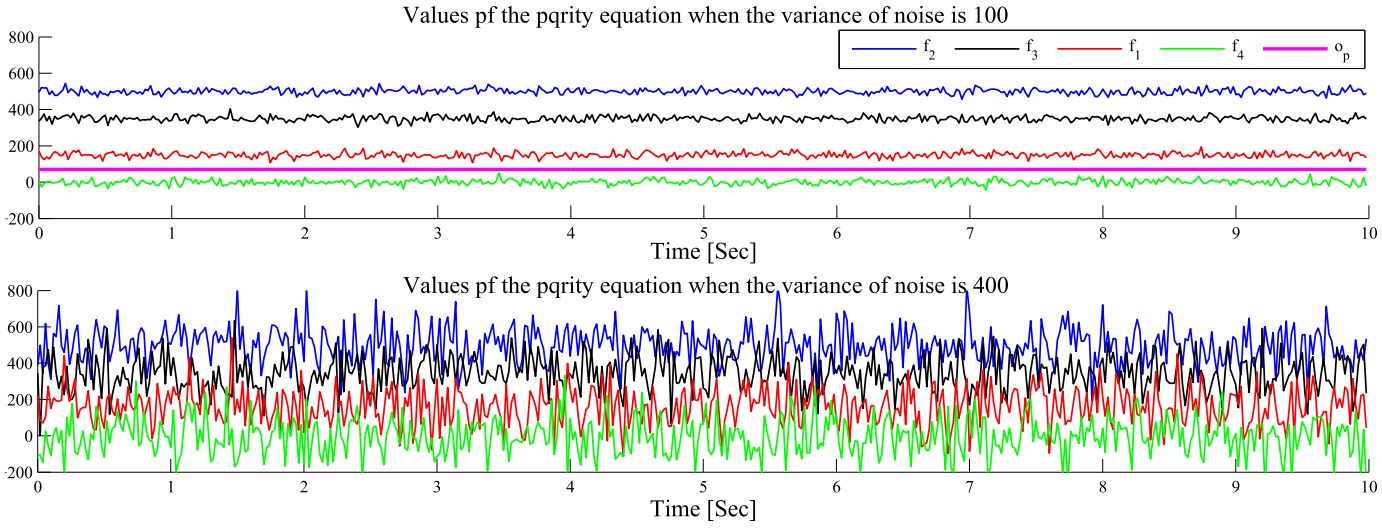

Fig. 5. The results based on parity equation. (For interpretation of the colors in the figure(s), the reader is referred to the web version of this article.)

5.1. Comparison of ranking results

1) The method based on parity equation: In [56], the core idea is to establish the parity equation $f(\theta_i, \theta_j, \theta_k, p_i, p_j, p_k)$ according to the aerodynamic model of FADS system.

$$f(\theta_i, \theta_j, \theta_k, p_i, p_j, p_k) = \begin{bmatrix} \cos^2\theta_k - \cos^2\theta_j \\ \cos^2\theta_i - \cos^2\theta_k \\ \cos^2\theta_j - \cos^2\theta_i \end{bmatrix}^T \begin{bmatrix} p_i \\ p_j \\ p_k \end{bmatrix} = 0.$$

However, this system inevitably exists measurement noise, that is, this equation cannot always hold. Thus, the threshold op based on engineering experience is adopted. As long as $f(\theta_i, \theta_j, \theta_k, p_i, p_j, p_k) < o_p$, the above equation is still considered to be approximately true and the flag bit is set to 0. Considering that there are four measurement taps researched in the paper, this means that there will be a total of $C_4^3 = 4$ flags, which are $f_1 = f(\theta_1, \theta_3, \theta_5, p_1, p_3, p_5)$, $f_2 = f(\theta_1, \theta_3, \theta_6, p_1, p_3, p_6)$, $f_3 = f(\theta_1, \theta_5, \theta_6, p_1, p_5, p_6)$, and $f_4 = f(\theta_3, \theta_5, \theta_6, p_3, p_5, p_6)$. After all the flag bits are obtained, the fault type is finally determined by comparing with the standard fault vector table in [56]. Therefore, whether a suitable o_p can be selected or not will directly affect the final fault detection results. For the purposes of this example, the values of the parity equation and op are shown in the top half of Fig. 5. As we can see, $o_p = 50$ is an advisable choice. However, once the noise variance of the system increases, The amplitude of $f(\theta_i, \theta_j, \theta_k, p_i, p_j, p_k)$ will absolutely increase with it. The result is shown in the lower half of Fig. 5 when the variance is 400. Obviously, all the data is mixed together and it is impossible to find a suitable o_p. Thus, the method is invalid.

2) The method based on χ^2 distribution: As for the method in [57], the calculation procedures can be summarized into two steps: 1) Determine the situation of system according to whether the sum of χ^2 is greater than 7.78. This particular number is chosen because of the characteristics of χ^2. Once $\chi^2(4) = 7.78$, the probability of failure is more than 90% and the system is basically deemed to fault; 2) Judge the specific fault type by excluding the taps one by one.

As shown in the left half of Fig. 6, the sum of χ^2 is more than 7.78 and the system is abnormal. In order to determine the specific fault taps, all the four measurement taps are excluded one by one, the left half of Fig. 6 plots the four typical situations. For example, the green curve shows the values of χ^2 after removing tap 1. The bar chart reveals that the tap 1 is the faulty one visually.

Nevertheless, similar to the parity equation, the accuracy of this method is also largely constrained by the variance of noise. This is because the stability of a series of data and the variance is negatively correlated. In other words, as the variance increases, the sum of squares after the normalization of the residuals will not particularly fit the distribution of $\chi^2(4)$, which will certainly affect the final measurement accuracy. As we can see from the right half of Fig. 6, although this method can detect the failure of system, it can not offer the specific fault taps.

3) The method based on OWA: The above two methods are by far the most widely used methods in the fault detection of FADS. To further illustrate the superiority of the proposed method, we try to consider the problem from the perspective of information fusion and make a detailed comparison. Among all the fusion methods, OWA is a classical and convincing method because of the simple calculation and high accuracy. It is an aggregation operator that provides a parameterized family of aggregation operators between the minimum and the maximum [67]. Assume that $f : R^n \to R$, $f(a_1, a_2, \cdots, a_n) = \sum_{j=1}^n w_j b_j$, where $W = (w_1, w_2, \cdots, w_n)^T$ represents the weight vector, $w_j \in [0, 1]$ and $\sum_{j=1}^n w_j = 1$. b_j is the jth largest in $(a_1, a_2, \cdots, a_n)$.

For the example in Section 5, a_0, a_{-1}, a_2, and a_{-1} are viewed as the four attributes. The core idea is to fuse the similarity between *Input* and the four attributes of IR^1, IR^2, IR^3, IR^4, and IR^5. The reason for this is that similarity can well reflect the degree of matching. For instance, if the similarity between *Input* and the four attributes of IR^1 is the greatest, then *Input* and IR^1 can be considered the closest and the fault detection result is "Tap 1 faults". The main calculation process can be divided into three steps: 1) Calculate the score

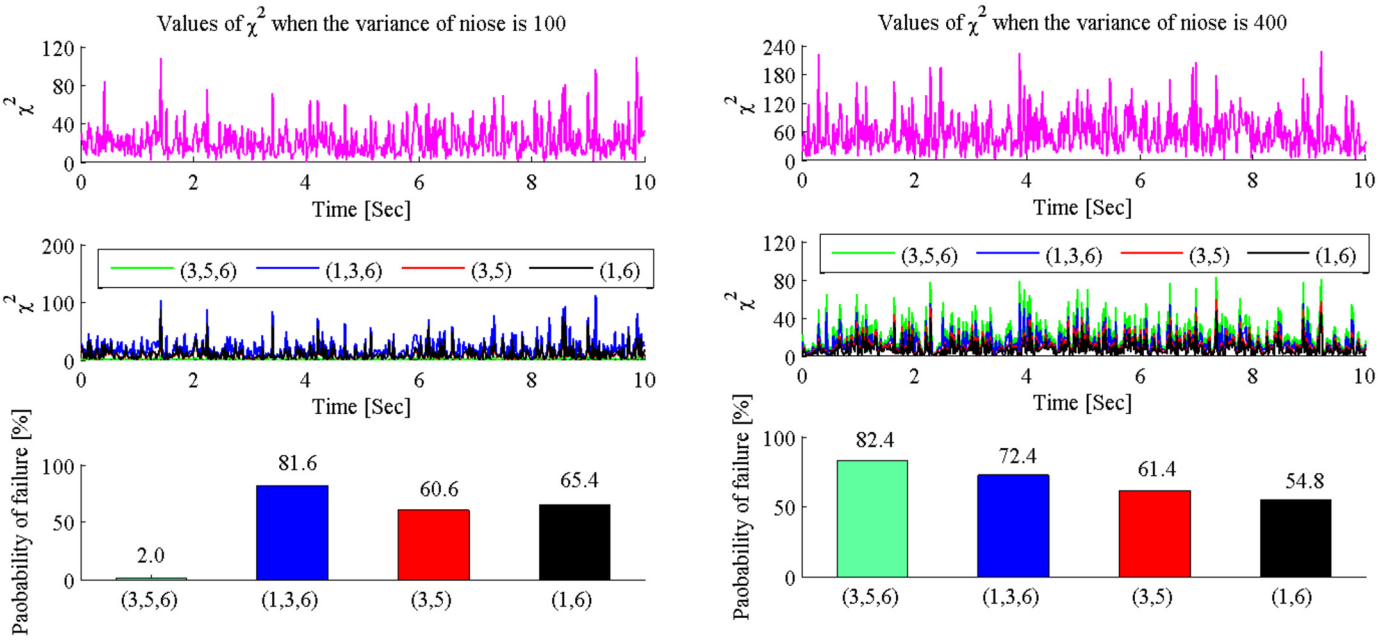

Fig. 6. The results based on χ^2 distribution.

Table 5
The score value of each IVNS.

Attributes \ Type	Tap 1 faults	Taps 1 and 6 fault	Taps 3 and 5 fault
a_0	0.0138	-0.1788	-0.0068
a_{-1}	0.0411	0.1912	0.0129
a_2	-0.1201	-0.1128	-0.0696
a_{-1}	0.1293	-0.1400	-0.0126

of each similarity in the form of IVNS in Table 3; 2) Integrate the score values of four attributes belonging to the same rule; 3) Regard the rule with the highest score as the final fault detection result.

The score of each IVNS can be derived by *Definition 16*, as shown in Table 5.

In the process of fusion, a crucial step is the determination of the weight vector. For OWA, a classic solution is fuzzy semantic quantization operator method proposed by Professor Zadeh in [68]:

$$w_i = Q\left[\frac{i}{n}\right] - Q\left[\frac{i-1}{n}\right], \quad i = 1, 2, \cdots, n \tag{27}$$

In this example, $n = 4$. Q represents the fuzzy semantic quantization operator and it can be calculated:

$$Q(r) = \begin{cases} 0, & r < \Upsilon \\ \frac{r-\Upsilon}{\varpi-\Upsilon}, & \Upsilon \le r \le \varpi \\ 1, & r > \varpi \end{cases} \tag{28}$$

where Υ and ϖ are two parameters, and can be determined according to the different principles. $\Upsilon, \varpi \in [0, 1]$. In [68,69], Herrera and Zadeh defined three fuzzy semantic quantization operators: "*Most*", "*At least half*", and "*As many as possible*". In these three cases, the parameters are set to $(\Upsilon, \varpi) = (0.3, 0.8)$, $(\Upsilon, \varpi) = (0, 0.5)$, and $(\Upsilon, \varpi) = (0.5, 1)$, respectively. The corresponding weight vectors are $W_1 = (w_1, w_2, w_3, w_4) = (0, 0.4, 0.5, 0.1)$, $W_2 = (w_1, w_2, w_3, w_4) = (0.5, 0.5, 0, 0)$, and $W_3 = (w_1, w_2, w_3, w_4) = (0, 0, 0.5, 0.5)$. To verify the effectiveness of OWA comprehensively, the three weight vectors are analyzed separately. The results are shown in Table 6. It can be seen that the fault detection results in the first two cases are correct. However, when $W_3 = (w_1, w_2, w_3, w_4) = (0, 0, 0.5, 0.5)$, the result is "Taps 3 and 5 fault", the method is invalid.

To fully analyze the differences of the six methods and prove the superiority of the proposed method, many repetitive digital simulations are carried out when variances are 100^2 Pa^2, 150^2 Pa^2, 200^2 Pa^2, 250^2 Pa^2, 300^2 Pa^2, 350^2 Pa^2, and 400^2 Pa^2. Results are shown in Fig. 7 and Table 7. With the increase of variance, the accuracy of all methods will decrease accordingly. But it can be seen that the accuracy of the proposed method can always maintain a high accuracy. The causes of these differences will be carefully analyzed in the following part.

Table 6
Fault detection results under different weight vectors.

	Tap 1 faults	Taps 1 and 6 fault	Taps 3 and 5 fault	
$W = (0, 0.4, 0.5, 0.1)$	0.0113	-0.1330	-0.0160	Tap 1 faults
$W = (0.5, 0.5, 0, 0)$	0.0852	0.0392	0.0031	Tap 1 faults
$W = (0, 0, 0.5, 0.5)$	-0.0532	-0.1594	-0.0411	Taps 3 and 5 fault

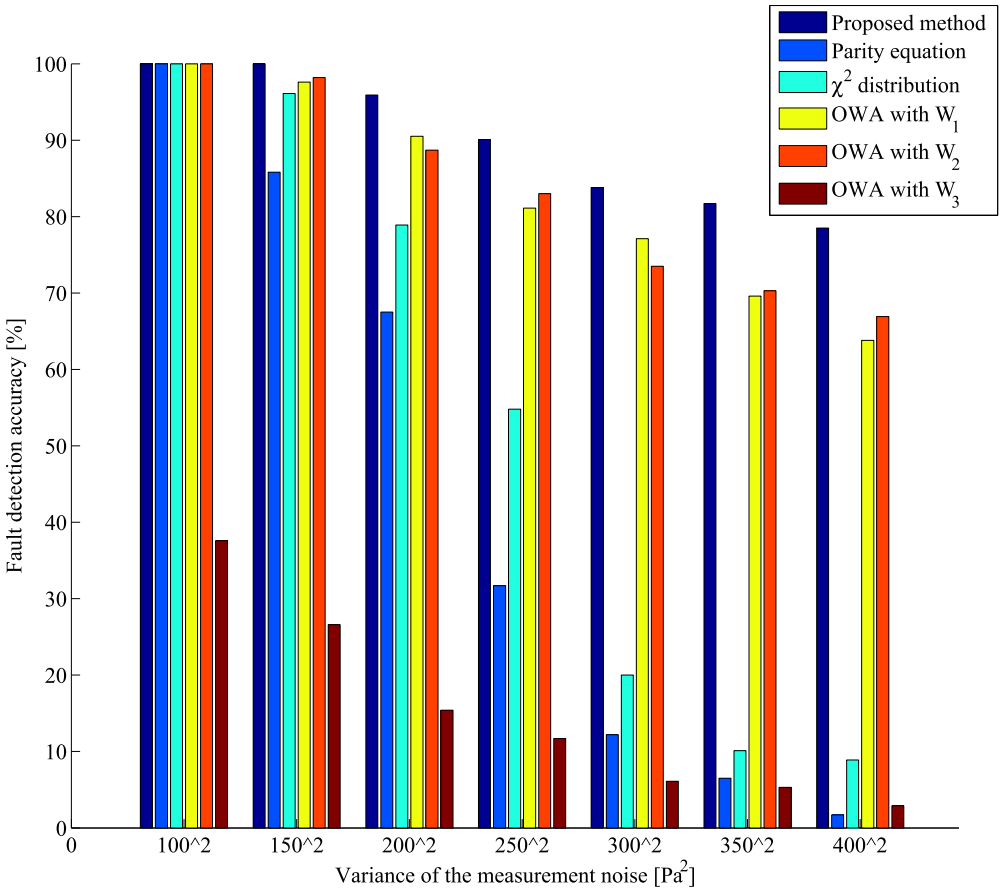

Fig. 7. Accuracy of the six methods under different variances.

Table 7
Accuracy of the six methods.

Methods / Variances [Pa^2]	Proposed method	Parity equation	χ^2 distribution	OWA with W_1	OWA with W_2	OWA with W_3
100	100%	100%	100%	100%	100%	37.6%
150	100%	85.8%	96.1%	97.6%	98.2%	26.6%
200	95.9%	67.5%	78.9%	90.5%	88.7%	15.4%
250	90.1%	31.7%	54.8%	81.1%	83.0%	11.7%
300	83.8%	12.2%	20.0%	77.1%	73.5%	6.1%
350	81.7%	6.5%	10.1%	69.6%	70.3%	5.3%
400	78.6%	1.7%	8.9%	63.8%	66.9%	2.9%

5.2. Discussion

For the proposed method, it is dedicated to solving the fault detection of FADS system from a new perspective. Compared with the model itself, we pay more attention to the uncertainty and randomness of results and incline to utilize IVNSs, BRB, and D-S evidence theory to describe the up-and-down results and consider the uncertainty and randomness of the system, rather than focusing on a single point. However, the system will encounter all kinds of unknown disturbances, that is, the model is uncertain. Therefore, the fault detection

methods based on the model are invalid while the proposed method shows strong robustness even if the fluctuation range of measurement results increase caused by the measurement noise. Although the method proposed in this paper does provide a new idea for solving the fault detection problem of FADS system, there are still some limitations: 1) some data is given on the basis of engineering experience when establish the BRB model; 2) The established model is not very accurate because of multiple disturbances and uncertainties. We will conduct relevant research based on extensive data in future.

6. Conclusion

In this paper, the fault detection problem has been investigated by combining IVNSs, BRB, and D-S evidence reasoning. Generally speaking, this paper makes five contributions with respect to the existing studies. First, IVNSs, BRB, and D-S evidence reasoning that all possess great power for addressing problems with random and uncertain information are firstly integrated. Next, a new approach of calculating the similarity between IVNSs is proposed. Furthermore, a new score function is put forward, which can get over the previous deficiencies. Finally, a high precision FADS model is established with the aerodynamic data obtained from the CFD software and the proposed algorithm is successfully applied to the fault detection of FADS. Results of numerical example show that the proposed method can address the fault detection problem efficiently. Compared with the existing methods, even on the condition of high variance, the proposed method will also have an excellent performance.

Declaration of competing interest

The authors declare that they have no known competing financial interests or personal relationships that could have appeared to influence the work reported in this paper.

Acknowledgements

This work is supported by the National Natural Science Foundation of China (No. 62073266 and No. 61374032). This work is supported by Shaanxi Province Key Laboratory of Flight Control and Simulation Technology.

References

[1] M. Kordestani, M. Saif, M. Orchard, R. Razavi-Far, K. Khorasani, Failure prognosis and applications-a survey of recent literature, IEEE Trans. Reliab. (2019) 1–21.
[2] Teymoor Ghanbari, Kalman filter based incipient fault detection method for underground cables, IET Gener. Transm. Distrib. 9 (14) (2015) 1988–1997.
[3] M. Miron, L. Frangu, S. Caraman, Actuator fault detection using extended Kalman filter for a wastewater treatment process, in: 2017 21st International Conference on System Theory, Control and Computing (ICSTCC), 2017.
[4] Y.L. Wang, T.B. Wang, W.W. Che, Active-varying sampling-based fault detection filter design for networked control systems, Math. Probl. Eng. 2014 (2014) 1–9.
[5] S. Gautam, P.K. Tamboli, V.H. Patankar, K. Roy, S.P. Duttagupta, Sensors incipient fault detection and isolation using Kalman filter and Kullback-Leibler divergence, IEEE Trans. Nucl. Sci. (2019) 1.
[6] P.P. Wang, Q. Yu, Y.J. Hu, C.X. Miao, Online detection of broken rotor bar fault in induction motors by combining estimation of signal parameters via min-norm algorithm and least square method, Chin. J. Mech. Eng. 30 (06) (2017) 1–11.
[7] T. Gush, S.B.A. Bukhari, R. Haider, S. Admasie, Y.S. Oh, G.J. Cho, C.H. Kim, Fault detection and location in a microgrid using mathematical morphology and recursive least square methods, Int. J. Electr. Power Energy Syst. 102 (November 2018) 324–331.
[8] A. Medvedev, Fault detection and isolation by a continuous parity space method, Automatica 31 (7) (1995) 1039–1044.
[9] Z. Sahar, N. Samsul, R.M. Mohammad, M. Mohammad, M. Norman, Broken rotor bar fault detection and classification using wavelet packet signature analysis based on Fourier transform and multi-layer perceptron neural network, Appl. Sci. 2018 (1) (2017).
[10] H. Xiaojia, X. Aidong, W. Kai, G. Haifeng, Z. Ning, L. Yang, H.S. Ho, Quadratic-wavelet-transform-based fault detection approach for temperature sensor, IEEJ Trans. Electr. Electron. Eng. (2018).
[11] M. Rezamand, M. Kordestani, R. Carriveau, S.K. Ting, M. Saif, An integrated feature-based failure prognosis method for wind turbine bearings, IEEE/ASME Trans. Mechatron. 99 (2020).
[12] H. Lala, S. Karmakar, Detection and experimental validation of high impedance arc fault in distribution system using empirical mode decomposition, IEEE Syst. J. 99 (2020) 1–12.
[13] S. Roshanmanesh, F. Hayati, M. Papaelias, Utilisation of ensemble empirical mode decomposition in conjunction with cyclostationary technique for wind turbine gearbox fault detection, Appl. Sci. Basel 31 (5) (2020).
[14] Z. Xu, C. Li, Y. Yang, Fault diagnosis of rolling bearing of wind turbines based on the variational mode decomposition and deep convolutional neural networks, Appl. Soft Comput. 95 (2020) 106515.
[15] Q. Yue, Fault detection and diagnosis of aero starter generator based on spectrum analyses, J. Bjing Univ. Aeronaut. Astronaut. (2004).
[16] J. Rangel-Magdaleno, H. Peregrina-Barreto, J. Ramirez-Cortes, I. Cruz-Vega, Hilbert spectrum analysis of induction motors for the detection of incipient broken rotor bars, Measurement (2017) S0263224117303792.
[17] S. Krishnannair, Fault detection of Tennessee Eastman process using kernel dissimilarity scale based singular spectrum analysis, IFAC-PapersOnLine 52 (29) (2019) 204–209.
[18] N. Chai, M. Yang, Y.Q. Li, D.G. Xu, Gearbox fault detection by Haar wavelet and envelope spectrum analysis of motor current, in: 2017 IEEE Transportation Electrification Conference and Expo, Asia-Pacific (ITEC Asia-Pacific), 2017.
[19] Y. Li, L. Wang, J. Guan, A spectrum detection approach for bearing fault signal based on spectral kurtosis, Shock Vib. 2017 (2) (2017) 1–9.
[20] X. Gong, W. Qiao, Bearing Fault Detection for Direct-Drive Wind Turbines via Stator Current Spectrum Analysis, 2011, pp. 313–318.
[21] C.F. Yan, H.B. Wang, L.L. Zhou, Z.X. Li, Fault diagnosis expert system of turbine generator sets based on rule reasoning and case reasoning, Appl. Mech. Mater. 513–517 (2014) 4443–4448.
[22] L. Wang, T.Z. Sui, Y. Song, H.X. Zhao, B.R. Zhuang, Research and implementation of an expert system for fault diagnosis of fan based on knowledge rule, Adv. Mater. Res. 201–203 (2011) 1989–1992.
[23] D. Ma, Y. Liang, X. Zhao, R. Guan, X. Shi, Multi-bp expert system for fault diagnosis of powersystem, Eng. Appl. Artif. Intell. 26 (3) (2013) 937–944.
[24] G.P. Li, Q.W. Zhang, Hydraulic fault diagnosis expert system of excavator based on fault tree, Adv. Mater. Res. 228–229 (2011) 439–446.
[25] A.Y. Zhang, X.G. Zhao, L. Zhang, General fault monitoring and diagnosis expert system based on fault tree and multi-sensor information, Appl. Mech. Mater. 121 (126) (2011) 4481–4485.
[26] Y. Youjun, L. Xiang, Z. Qun, Developmentof automobile fault diagnosis expert system based on fault tree — neural network ensamble, in: International Conference on Electronics, 2011.
[27] J.X. Zou, Y. Zhang, G. Zheng, The missile fault diagnosis expert system based on ga-bpnn, Adv. Mater. Res. 255 (260) (2011) 2164–2168.
[28] H. Monsef, A.M. Ranjbar, S. Jadid, Fuzzy rule-based expert system for power system fault diagnosis, IEE Proc., Gener. Transm. Distrib. 144 (2) (1997) 186–192.

[29] D. Qiu, J.M. Zhang, The application of mechanical failure diagnosis expert system for the improvement of vibration fault monitor and diagnosis based on rough set theory, Adv. Mater. Res. 461 (2012) 191–195.
[30] X. Xu, D. Cao, Y. Zhou, J. Gao, Application of neural network algorithm in fault diagnosis of mechanical intelligence, Mech. Syst. Signal Process. 141 (2020) 106625.
[31] B.T. Thumati, M.A. Feinstein, S. Jagannathan, A model-based fault detection and prognostics scheme for Takagi–Sugeno fuzzy systems, IEEE Trans. Fuzzy Syst. 22 (4) (2014) 736–748.
[32] M.U. Hong-Lei, C. Yong-Mei, G. Bin, L. Jian-Xin, L.I. Song, S.O. Automation, N.P. University, Method of joint fault detection based on evidential reasoning, Control Decis. (2016).
[33] F.U. Hua, L. Ming-Guang, K. Hai-Chao, Based on principal component analysis and d-s evidence theory and application of sensor fault diagnosis, Appl. Res. Comput. (2011).
[34] W. Sun, W. Li, Avionic devices fault diagnosis based on fusion method of rough set and d-s theory, J. Bjing Univ. Aeronaut. Astronaut. (2015).
[35] X. Ji, Y. Ren, H. Tang, C. Shi, J. Xiang, An intelligent fault diagnosis approach based on Dempster-Shafer theory for hydraulic valves, Measurement (2020) 108129.
[36] H. Zhu, Z. Ma, H. Sun, H. Wang, Information correlation entropy based d-s evidence theory used in fault diagnosis, in: Quality, Reliability, Risk, Maintenance, and Safety Engineering (ICQR2MSE), 2012 International Conference on, 2012.
[37] S. Yanan, Fault diagnosis study based on neural network and d-s evidence theory, Chin. J. Ship Res. (2008).
[38] L. Zhang, Y. Dong, Research on diagnosis of ac engine wear fault based on support vector machine and information fusion, J. Comput. 7 (9) (2012) 701–709.
[39] Z. Chenglin, S. Xuebin, S. Songlin, J. Ting, Fault diagnosis of sensor by chaos particle swarm optimization algorithm and support vector machine, Expert Syst. Appl. 38 (8) (2011) 9908–9912.
[40] X. Tang, L. Zhuang, J. Cai, C. Li, Multi-fault classification based on support vector machine trained by chaos particle swarm optimization, Knowl.-Based Syst. 23 (5) (2010) 486–490.
[41] X. Li, S. Wu, X. Li, H. Yuan, D. Zhao, Particle swarm optimization-support vector machine model for machinery fault diagnoses in high-voltage circuit breakers, Chin. J. Mech. Eng. 33 (1) (2020) 6.
[42] D.L. Yang, X.J. Li, K. Wang, L.L. Jiang, Support vector machine optimization based on bacterial foraging algorithm and applied in fault diagnosis, Adv. Mater. Res. 216 (2011) 153–157.
[43] L. Zhong, Z. Qiang, Z. Kun, C. Li, S. Shuangkui, Fault diagnosis of transformer based on extreme learning machine optimized by genetic algorithm, High Volt. Appar. 51 (8) (2015) 49–53.
[44] X. Lin, S. Ke, Z. Li, H. Weng, X. Han, A fault diagnosis method of power systems based on improved objective function and genetic algorithm-tabu search, IEEE Trans. Power Deliv. 25 (3) (2010) 1268–1274.
[45] C. Yang, Multiple soft fault diagnosis of analog filter circuit based on genetic algorithm, IEEE Access 99 (2020) 1.
[46] C.H. Lo, Y.K. Wong, A.B. Rad, K.M. Chow, Fusion of qualitative bond graph and genetic algorithms: a fault diagnosis application, ISA Trans. 41 (4) (2002) 445–456.
[47] Q. Yang, D. Zhang, J. Zhuang, F. Sun, J. Wang, Fault diagnosis method using support vector machine with improved complex system genetic algorithm, J. Vibroeng. 15 (3) (2013) 1147–1156.
[48] W.Q. Zhao, R. Cai, L.W. Wang, D.W. Wang, Fault diagnosis of wind turbine gearbox based on least square support vector machine with genetic algorithm, Adv. Mater. Res. 846–847 (2014) 620–623.
[49] L.Y. Song, H.Q. Wang, J. Pan, J.J. Gao, K. Li, Application of ant colony algorithm in fault diagnosis of roller bearing, Adv. Mater. Res. 291–294 (2011) 1957–1960.
[50] X.L. Zhang, X.F. Chen, Z.J. He, Fault diagnosis based on support vector machines with parameter optimization by an ant colony algorithm, Proc. Inst. Mech. Eng., Part C, J. Mech. Eng. Sci. 224 (1) (2010) 217–229.
[51] L. Wang, Q. Niu, M. Fei, A novel quantum ant colony optimization algorithm and its application to fault diagnosis, Trans. Inst. Meas. Control 30 (3–4) (2008) 313–329.
[52] L.C. Echevarria, O.L. Santiago, J.A.H. Fajardo, A.J.S. Neto, D.J. Sanchez, A variant of the particle swarm optimization for the improvement of fault diagnosis in industrial systems via faults estimation, Eng. Appl. Artif. Intell. 28 (Feb. 2014) 36–51.
[53] Y. He, W.J. Ma, J.P. Zhang, J.C.M. Kao, W.P. Sung, The parameters selection of pso algorithm influencing on performance of fault diagnosis, MATEC Web Conf. 63 (2016).
[54] L. Yixiao, Z. Lei, L. Weihua, Regrouping Particle Swarm Optimization Based Variable Neural Network for Gearbox Fault Diagnosis, 2017, pp. 1–10.
[55] B.R. Han, S.X. Liu, L.S. Cai, Particle swarm neural network in application of soft fault diagnosis of analog circuit, Adv. Mater. Res. 694–697 (2013) 1349–1353.
[56] G. Yang-Ming, L.I. Qing-Dong, C. Xiao-Bin, Z. Zheng-Jun, Fads sensors fault detection based on parity equation, Aeronaut. Comput. Tech. (2010).
[57] Z. Shouduo, L. Yuping, Y. Wei, Technology research of fads system fault detection and management based on χ^2 analysis, Comput. Meas. Control (2007).
[58] J. Ye, Similarity measures between interval neutrosophic sets and their applications in multicriteria decision-making, J. Intell. Fuzzy Syst. 26 (1) (2014) 165–172.
[59] C. Jiqian, Y. Jun, D. Shigui, Vector similarity measures between refined simplified neutrosophic sets and their multiple attribute decision-making method, Symmetry 9 (8) (2017) 1–13.
[60] J. Ren, Y. Gao, Discrete fuzzy-stochastic multi-criterion decision-making method with incomplete information, Xitong Gongcheng Lilun Yu Shijian/Syst. Eng. Theory Pract. 31 (1) (2011) 122–130.
[61] H.Y. Zhang, J.Q. Wang, X.H. Chen, Interval neutrosophic sets and their application in multicriteria decision making problems, Sci. World J. (2014) 1–15.
[62] G.L. Tang, Approaches for Relational Multiple Attribute Decision Making with Interval Neutrosophic Numbers Based on Choquet Integral, Shandong University, 2016.
[63] Peide Liu, Ridvan Sahin, Maximizing deviation method for neutrosophic multiple attribute decision making with incomplete weight information, Neural Comput. Appl. (2016).
[64] L.S. Jin, Vector t-norms with applications, IEEE Trans. Fuzzy Syst. 25 (99) (2016) 1644–1654.
[65] Y.B. Liu, D.B. Xiao, Trade-off design of measurement tap configuration and solving model for a flush air data sensing system, Measurement 90 (2016) 278–285.
[66] G. Chen, B. Chen, P. Li, P. Bai, C. Ji, Study on algorithms of flush air data sensing system for hypersonicvehicle, Proc. Eng. 99 (2015) 860–865.
[67] R.R. Yager, On ordered weighted averaging aggregation operators in multicriteria decisionmaking, IEEE Trans. Syst. Man Cybern. (1988).
[68] L.A. Zadeh, A computational approach to fuzzy quantifiers in natural languages, Comput. Lingus (1983) 149–184.
[69] F. Herrera, E. Herrera-Viedma, L. Martínez, A fusion approach for managing multi-granularity linguistic term sets in decision making, Fuzzy Sets Syst. 114 (1) (2000) 43–58.